

Low-light Image Enhancement by Retinex Based Algorithm Unrolling and Adjustment

Xinyi Liu, Qi Xie, Qian Zhao, Hong Wang and Deyu Meng

School of Mathematics and Statistics, Xi'an Jiaotong University, 28 West Xianning Road, Xi'an, 710049, Shaanxi, P.R. China.

Contributing authors: xlyqnhqs98@stu.xjtu.edu.cn; xie.qi@xjtu.edu.cn; timmy.zhaoqian@xjtu.edu.cn; hongwang01@stu.xjtu.edu.cn; dymeng@xjtu.edu.cn;

Abstract

Motivated by their recent advances, deep learning techniques have been widely applied to low-light image enhancement (LIE) problem. Among which, Retinex theory based ones, mostly following a decomposition-adjustment pipeline, have taken an important place due to its physical interpretation and promising performance. However, current investigations on Retinex based deep learning are still not sufficient, ignoring many useful experiences from traditional methods. Besides, the adjustment step is either performed with simple image processing techniques, or by complicated networks, both of which are unsatisfactory in practice. To address these issues, we propose a new deep learning framework for the LIE problem. The proposed framework contains a decomposition network inspired by algorithm unrolling, and adjustment networks considering both global brightness and local brightness sensitivity. By virtue of algorithm unrolling, both implicit priors learned from data and explicit priors borrowed from traditional methods can be embedded in the network, facilitate to better decomposition. Meanwhile, the consideration of global and local brightness can guide designing simple yet effective network modules for adjustment. Besides, to avoid manually parameter tuning, we also propose a self-supervised fine-tuning strategy, which can always guarantee a promising performance. Experiments on a series of typical LIE datasets demonstrated the effectiveness of the proposed method, both quantitatively and visually, as compared with existing methods.

Keywords: Low-light image enhancement, Retinex theory, Deep learning, Algorithm unrolling.

1 Introduction

Due to the lack of sufficient amount of light, photos taken under low-light environment suffer from various of degradations, such as low visibility, color biases and noise. These unexpected degradations not only reduce the user experience of consumer photography, but also degrade the performance of downstream vision tasks (J. Liu, Xu, Yang, Fan, & Huang, 2021) in industrial purpose, including object detection (Zhao, Zheng, Xu,

& Wu, 2019) and tracking (Wu, Lim, & Yang, 2015). Therefore, it is indispensable to enhance the images captured under low-light conditions for further utilization. In the last decades, there are various methods have been developed for this low-light image enhancement (LIE) problem, including both traditional methods and deep learning based ones.

In the early years, LIE was achieved by traditional image processing techniques, specifically

value mapping methods, such as histogram equalization (HE) (Acharya & Ray, 2005; Kim, 1997; Pisano et al., 1998; Pizer et al., 1987; Reza, 2004; C.-C. Sun, Ruan, Shie, & Pai, 2005; Zuiderveld, 1994) and gamma correction (GC) (Guan, Jian, Hongda, Zhiguo, & Haibin, 2009; Huang, Cheng, & Chiu, 2012; Singh, Kumar, Balyan, & Singh, 2017; W. Wang, Sun, & Ng, 2019). The main idea behind these methods is applying certain transformation to the pixel values of the observed low-light image, in order to stretch the dynamic range of it. However, these methods intrinsically try to enhance the contrast of the images, rather than directly adjust the illumination, and also neglect other degradations, such as noise, leading to inferior performance.

Later, model based methods become more popular, which assume that the low-light image is obtained following a physical observation model, and then enhance the image based on it. Most powerful methods along this line motivated their observation models from the well-known Retinex theory (Land, 1977), where the basic assumption is that the observed image can be decomposed into reflectance and illumination layers, while both the low-light image and the corresponding normal-light one share the same reflectance layer. Therefore, one can first do such a decomposition to the low-light image (or only estimate the illumination layer), and then directly recover the reflectance layer as the final result (Jobson, Rahman, & Woodell, 1997; Rahman, Jobson, & Woodell, 1996), or further adjust the illumination layer to enhance the image (S. Wang, Zheng, Hu, & Li, 2013a). The key to such methods is designing proper priors for images or their decompositions, and various effective priors have been considered, including dark channel prior (X. Guo, 2016), sparse gradient prior (Fu, Zeng, Huang, Zhang, & Ding, 2016), structure-revealing prior (M. Li, Liu, Yang, Sun, & Guo, 2018a) and low-rank prior (Ren, Yang, Cheng, & Liu, 2020). In addition to Retinex theory, there are also other observation models having been considered. For example, in some studies, the authors treated LIE as the inverted dehazing problem (L. Li, Wang, Wang, & Gao, 2015; X. Zhang, Shen, Luo, Zhang, & Song, 2012), and thus constructed algorithms based on the atmospheric scattering model (Narasimhan & Nayar, 2002). These model based methods, however, highly rely on the hand-crafted

priors for images or their decompositions, which largely limits their performance.

Inspired by recent advances of deep neural networks (DNNs) in low-level computer vision (Dong, Loy, He, & Tang, 2015; K. Zhang, Zuo, Chen, Meng, & Zhang, 2017), deep learning based methods have also been developed for LIE. Among them, there are mainly two methodologies in applying deep learning to LIE. The first is to learn a direct mapping, parameterized by a DNN, from the low-light image to the corresponding normal-light one (Lore, Akintayo, & Sarkar, 2017; Lv, Lu, Wu, & Lim, 2018; Ma, Liu, Zhang, Fan, & Luo, 2021; Xu, Yang, Yin, & Lau, 2020), regardless of the physical model underlying the low-light observation. The second is introducing Retinex theory to the network designing (R. Liu, Ma, Zhang, Fan, & Luo, 2021; Shen et al., 2017; Y. Wang et al., 2019a; W. Yang, Wang, Fang, Wang, & Liu, 2020), in which the DNN firstly tries to decompose the low-light image into two components, i.e., reflectance and illumination, and then doing postprocessing (possibly achieved also by a DNN) (Y. Zhang, Guo, Ma, Liu, & Zhang, 2021) or directly using the reflectance layer as the final result (C. Li, Guo, Porikli, & Pang, 2018; R. Wang et al., 2019), inheriting the similar idea as that of traditional Retinex based methods. Comparatively, Retinex inspired methods have attracted more attention, since they generally incorporate more prior knowledge by the physical observation model, and thus are expected to be more effective.

Though progress has been continuously made, the performance of current DNNs for LIE is still not significant, compared with their applications to other image restoration or enhancement tasks, such as image denoising and super-resolution, due to relatively more complicated degradations involved in low-light images. After comprehensively investigating current deep learning based LIE studies, we find one major issue possibly leading to such lower-than-expected performance of DNNs, that more attention is paid to fancy and powerful modules in designing the network architectures, while many valuable experiences from traditional methods are ignored, especially from the ones inspired by Retinex theory. This deficiency not only leads to less interpretability of DNNs, but could also limit their performance. We have noticed that there are studies concerning this

issue (R. Liu et al., 2021), but current investigations are still not sufficient and have large room for improvement. Besides, as a post-processing step in using Retinex model, adjusting one or both of the decomposed reflectance and illumination is important. However, current studies either resort to traditional image processing techniques, such as Gamma Correction, or design relatively complicated network, for this goal, both of which are not very satisfactory in practice.

To address the aforementioned issues, in this paper we propose an effective and interpretable DNN for LIE, by fully considering useful experiences from traditional Retinex methods, and carefully designing the adjusting modules for the decomposed image layers. Specifically, following the pipeline that has been shown to be effective (Y. Zhang et al., 2021), we propose a DNN that firstly decompose the image into reflectance and illumination layers, and then adjusting both of them to obtain the final enhancement results:

- For the decomposition, we design the network architecture inspired by unrolling the optimization procedure for solving an Retinex based image decomposition model. Different from the previous study that also considered the algorithm unrolling of an Retinex based optimization (R. Liu et al., 2021), while constructed the network with neural architecture search, we pay more attention to the algorithm inspired operations with more sophisticated prior borrowed from traditional methods. To be specific, in addition to implicit priors that can be learned by network as many other unrolling type DNN, we introduce the structure-revealing prior (M. Li et al., 2018a; Ren et al., 2020) specifically designed for the LIE problem to the network. This strategy on the one hand takes the superiority of data-driven methods in flexibly prior learning, and on the other hand also naturally inherits the advantageous experience from traditional methods.
- For the adjustment, we design simple yet effective networks, which integrate global brightness and local brightness sensitivity, for illumination and reflectance, respectively. The physical mechanism of the proposed adjustment networks is also relatively easier to explain, as compared with existing methods.
- Besides, as a supplement to user-controlled enhancement level, we also propose a self-supervised strategy to fine-tune the adjustment networks at test time. This self-supervised fine-tuning strategy can generally produce a satisfactory result, without user intervention.

All of these advantages have been substantiated by comprehensive experiments on typical LIE datasets.

The paper is organized as follows. In Section 2, we review related work on the studied problem. Section 3 presents the details of the proposed framework for LIE. In Section 4, extensive experimental results on typical LIE datasets are introduced to demonstrate the superiority of the proposed method. The conclusion is finally made in Section 5.

2 Related Work

In this section, we review related work on the LIE problem. Our main focus is on Retinex theory based methods, both traditional and deep learning ones, while interested readers could refer to (J. Liu et al., 2021) for a more comprehensive review.

2.1 Traditional Methods

2.1.1 Value Mapping Methods

The early attempts for the LIE problem are mainly focused on value mapping in traditional image processing techniques, such as Histogram Equalization (HE) (Hummel, 1977) and Gamma Correction (GC). The main idea of HE type methods (Acharya & Ray, 2005; Kim, 1997; Pisano et al., 1998; Pizer et al., 1987; Reza, 2004; C.-C. Sun et al., 2005; Zuiderveld, 1994) is to enhance images by mapping the histogram distribution of an image to approximately a uniform one. Different from HE, GC type methods (Guan et al., 2009; Huang et al., 2012; Singh et al., 2017; W. Wang et al., 2019) realize image enhancement by nonlinear editing of its gamma curve, which results in change to the tone of the image. There are also studies that used different value mappings. For example, Yuan and Sun (2012) considered region-level illumination and applied a detail-preserved S-curve adjustment to enhance exposure. Generally, these methods are too specific with less flexibility to real

scenarios, and tend to amplify noise existing in low-light images.

2.1.2 Retinex Theory Based Methods

Retinex theory (Land, 1977) plays an important role in traditional model-based LIE methods. The key step of applying Retinex theory is to decompose the image into reflectance and the illumination layers, representing the reflected objects and the light shining on the surface of objects, respectively. Such a Retinex decomposition can be achieved by traditional image processing techniques, such as filtering (Jobson et al., 1997; Rahman et al., 1996; S. Wang, Zheng, Hu, & Li, 2013b). However, such methods did not take sophisticated image priors into considerations, and thus the performance is not satisfactory. A more preferable way in using Retinex theory is to formulate the Retinex decomposition as an optimization problem. However, since the solution to Retinex decomposition is mathematically non-unique, it is crucial to design proper priors to make the optimization well-defined. Along this line, multiple priors have been adopted or newly designed. For example, Guo (2016) used the dark channel prior for images and sparse gradient prior to illumination; Fu et al. (2016) proposed to consider sparse gradient prior to reflectance while smoothness prior to illumination; Li et al. (2018a) designed a structure-revealing prior for reflectance while also considered the robustness issue; Ren et al. (2020) improved the model in (M. Li et al., 2018a) by introducing low-rank prior to similar patches extracted from reflectance. These methods, however, highly rely on the hand-crafted priors for images or their decompositions, which tends to limit their performance.

2.2 Deep Learning Based Methods

2.2.1 Retinex Inspired Deep Learning Methods

Inspired by its successful applications in traditional LIE methods, Retinex theory has also been adopted in deep learning era, and there are mainly two methodologies in applying it. The first is to directly treat the estimated reflectance layer (can be achieved by first estimating the illumination and then doing element-wise division) as the enhanced image. For example, Shen et al.

(2017) simulated multi-scale Retinex with a convolution neural network; Li et al. (2018) proposed an improved network framework for correcting the illumination; Wang et al. (2019b) designed a network to do Retinex decomposition in a progressive way; Wang et al. (2019) addressed this problem with the help of a down-sample image; Lv et al. (2020) built a noise compression network for reflectance denoising; Liu et al. (2021) proposed a Retinex inspired unrolling scheme with network architecture search (NAS). However, as analyzed in (Lu & Zhang, 2020), directly treating the reflectance might not be very reasonable, and therefore the second methodology, that additionally takes illumination adjustment into consideration, has also been adopted in many studies. For example, Chen et al. (2018) introduced additional feature extraction process for illumination mapping; Zhang et al. (2019) constructed an LIE processing pipeline, which first decomposes the image and then adjusts both the reflectance and illumination layers, and later improved it (Y. Zhang et al., 2021); Fan et al. (2020) considered the semantic information for better decomposition; Yang et al. (2021) introduced the sparse gradient regularization for the balance between details preservation and noise removal; Ma et al. (2021) designed a context-sensitive decomposition module and used spatially varying illumination guidance for estimation.

Above methods were all built in a fully supervised fashion, and there are also some recent studies on unsupervised learning. For example, Zhao et al. (2021) built Retinex-DIP model by combining the Retinex model and deep image prior (Ulyanov, Vedaldi, & Lempitsky, 2018); Zhu et al. (2020) proposed RRDNet by training the network in a zero-shot way with specifically designed loss functions.

The current Retinex inspired deep learning studies, however, mostly try to build their inference architecture with fancy modules, while ignore advantageous experiences from traditional ones, and thus still has room to improve. It should be mentioned that, there has been an attempt to this issue (R. Liu et al., 2021), but it still did not fully make use of the useful priors in the optimization based Retinex decomposition models.

2.2.2 Other Deep Learning Methods

There are deep learning based methods that did not make use of Retinex theory. For example, Lore et al. (2017) designed an autoencoder structure to learn a direct mapping from low-light image to the corresponding normal-light one; Lv et al. (2018) built a multi-branch network for this task; Lim and Kim (2020) introduced Laplacian pyramid to a multi-scale structure for better feature extraction; Zheng et al. (2021) presented an algorithm unrolling scheme mainly focusing on denoising.

Unsupervised and semi-supervised methodologies have also been considered. For example, Jiang et al. (2021) proposed a GAN-based framework for LIE; Guo et al. (2020) put forward a zero-shot method, inspired by curve adjusting for light enhancement, which was later extended (C. Li, Guo, & Loy, 2021); Yang et al. (2020) introduced unpaired data in addition to paired ones in a semi-supervised fashion.

These non-Retinex methods can also achieve promising results due to the power of DNNs, but are generally with less interpretability compared with those Retinex inspired ones.

3 Proposed Approach

3.1 Overview of Proposed Framework

3.1.1 Retinex Theory and LIE

For an observed image, denoted as $\mathbf{I} \in \mathbb{R}^{H \times W}$, it can be decomposed into two components based on Retinex theory (Land, 1977) as

$$\mathbf{I} = \mathbf{R} \circ \mathbf{L}, \quad (1)$$

where $\mathbf{R} \in \mathbb{R}^{H \times W}$ denotes the reflectance layer, $\mathbf{I} \in \mathbb{R}^{H \times W}$ represents the illumination layer, and \circ means the element-wise product¹. The key assumption of Retinex theory is that, ideally, images taken under the same scene, with different light conditions, can have different illumination layers, while share the same reflectance layer.

¹Note that for color image, both \mathbf{I} and \mathbf{R} have three channels, and (1) should be more rigorously written as $\mathbf{I}^c = \mathbf{R}^c \circ \mathbf{L}$, $c \in \{r, g, b\}$. In the remaining of this paper, we mainly discuss with one-channel image for notation simplicity, if not emphasized. Nevertheless, the discussions can be straightforwardly extended to color image, on which our proposed framework indeed operates.

According to this theory, for the LIE problem, if such a decomposition for the low-light image can be accurately estimated, its enhancement can be obtained correspondingly. Specifically, suppose low-light image \mathbf{I}_l can be decomposed into reflectance \mathbf{R} and illumination \mathbf{L}_l , and then there are two possible ways to obtain the enhanced image $\hat{\mathbf{I}}_{\text{en}}$:

- Let $\hat{\mathbf{I}}_{\text{en}} = \mathbf{R}$, or equivalently $\hat{\mathbf{I}}_{\text{en}} = \mathbf{I}_l \oslash \mathbf{L}_l$, where \oslash denotes the element-wise divide.
- Adjust \mathbf{L}_l to $\hat{\mathbf{L}}_h$ (as an approximation to groundtruth illumination \mathbf{L}_h of normal-light image), and then let $\hat{\mathbf{I}}_{\text{en}} = \mathbf{R} \circ \hat{\mathbf{L}}_h$.

As discussed in (X. Guo, 2016; Lu & Zhang, 2020), the first approach, though works, is less physically reasonable, since illumination is also an important factor to human perception (Lu & Zhang, 2020). Therefore, we focus on the second one, and the following discussions are also based on it, if not emphasized.

In real scenarios, however, the estimated reflectance $\hat{\mathbf{R}}_l$ of the low-light image may contain unexpected degradations (Fan et al., 2020; Y. Zhang et al., 2021), such as noise and contrast biases, and thus not necessarily equals to the ideal reflectance \mathbf{R} . Therefore, adjustment to $\hat{\mathbf{R}}_l$ is also important. Consequently, Retinex theory based LIE can be summarized as the following steps:

- Decompose the low-light image to reflectance and illumination layers, such that

$$\mathbf{I}_l \approx \hat{\mathbf{R}}_l \circ \hat{\mathbf{L}}_l. \quad (2)$$

- Adjust both the reflectance and illumination layers, which can be expressed as

$$\begin{cases} \hat{\mathbf{R}}_{\text{adj}} = f_R(\hat{\mathbf{R}}_l), \\ \hat{\mathbf{L}}_{\text{adj}} = f_L(\hat{\mathbf{L}}_l). \end{cases} \quad (3)$$

where, $f_R(\cdot)$ and $f_L(\cdot)$ denote the adjustment operations for reflectance and illumination layers, respectively.

- Recompose the reflectance and illumination to obtain the enhanced image by

$$\hat{\mathbf{I}}_{\text{en}} = \hat{\mathbf{R}}_{\text{adj}} \circ \hat{\mathbf{L}}_{\text{adj}}. \quad (4)$$

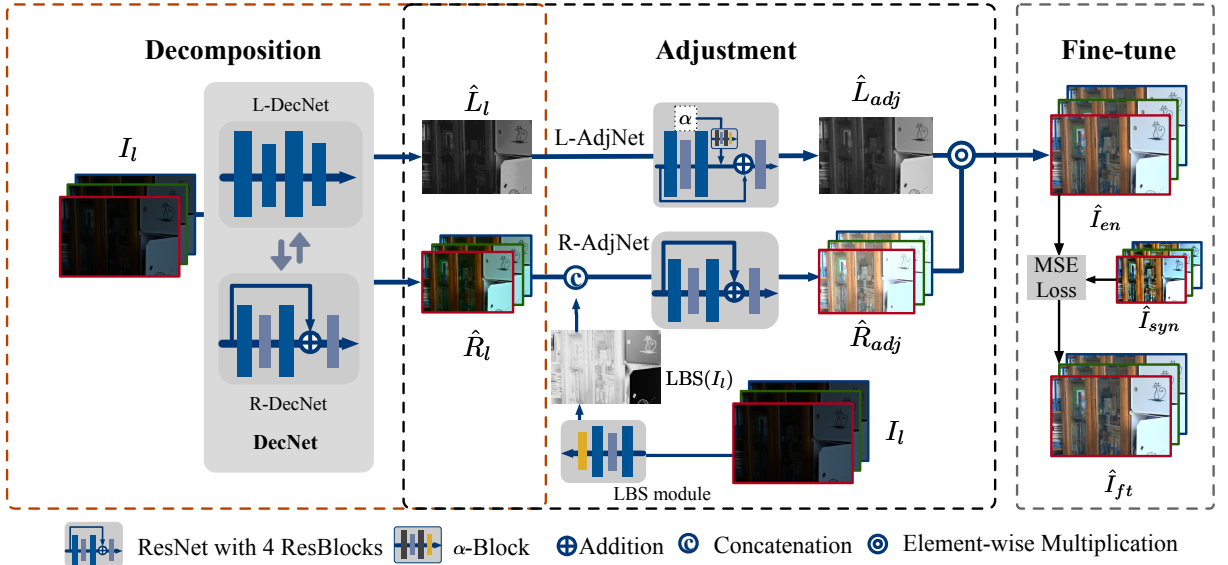


Fig. 1 Illustration of the proposed LIE framework.

3.1.2 Proposed Solution to Retinex Based LIE

Following the Retinex based LIE pipeline discussed above, the key is how to decompose the low-light image and adjust the decomposition results, which turns to designing effective network architectures for doing decomposition and adjustment, from deep learning perspective. We briefly introduce our solution to this as follows.

For decomposition, considering that most of existing deep learning methods did not fully make use of the experiences from traditional methods, we design a network inspired by algorithm unrolling of a Retinex based optimization model. This unrolling scheme can encode both the explicit prior, which has shown to be effective in traditional methods, and implicit prior, which can be learned by DNNs in a data-driven way. For adjustment, we design relatively simple and intuitively interpretable, yet effective modules to adjust the reflectance and illumination layers, respectively. In addition, we also introduce a self-supervised fine-tuning strategy as an optional post-processing step when doing inference. By this fine-tuning, a promising performance can generally be guaranteed, without much user intervention.

The overall framework of our method is illustrated in Fig. 1, and in the following subsections, we will discuss the details of each component, together with training strategies.

3.2 Retinex-based Decomposition Network

Recently, the algorithm unrolling methodology has attracted much attention, and been successfully applied to many low-level vision tasks (H. Wang, Xie, Zhao, & Meng, 2020; Xie, Zhou, Zhao, Xu, & Meng, 2020; D. Yang & Sun, 2018; Y. Yang, Sun, Li, & Xu, 2020; J. Zhang, Pan, Lai, Lau, & Yang, 2017). This network designing methodology on the one hand makes the DNN more explainable, since each stage can be related to one iteration in solving an optimization problem; and on the other hand can often enhance the performance of a specific task, since the inference goal can be done in a progressive way by the network, and implicit prior can be learned in a data-driven manner. Therefore, we also design our network inspired by algorithm unrolling, aiming at a better image decomposition.

3.2.1 Retinex-based Optimization Model for Image Decomposition

To design a DNN by algorithm unrolling, we first need to construct the optimization model for the concerned problem. For LIE, the general Retinex based optimization can be formulated as

$$\min_{\mathbf{R}, \mathbf{L}} \frac{1}{2} \|\mathbf{I} - \mathbf{R} \circ \mathbf{L}\|_F^2 + g_1(\mathbf{L}) + g_2(\mathbf{R}), \quad (5)$$

where $g_1(\cdot)$ and $g_2(\cdot)$ are regularizations to characterize the prior knowledge for illumination \mathbf{L} and reflectance \mathbf{R} , respectively, such that the Retinex decomposition is well-defined (note that decomposition $\mathbf{I} = \mathbf{R} \circ \mathbf{L}$ is not unique). Then one can unroll the iterative algorithm for solving this optimization, and implicitly embed each of the priors $g_1(\cdot)$ and $g_2(\cdot)$ to a network module, respectively. Such a strategy has been adopted in earlier work (R. Liu et al., 2021) that also considered algorithm unrolling based DNN for LIE.

In this work, we take a step further by adding an explicit prior term to the objective function in (5):

$$\begin{aligned} \min_{\mathbf{R}, \mathbf{L}} \frac{1}{2} \|\mathbf{I} - \mathbf{R} \circ \mathbf{L}\|_F^2 + g_1(\mathbf{L}) + g_2(\mathbf{R}) \\ + \frac{\gamma}{4} \sum_{i=x,y} \|\mathbf{d}_i \otimes \mathbf{R} - \mathbf{G}_i\|_F^2, \end{aligned} \quad (6)$$

where $\mathbf{d}_x = [1, 0, -1]^\top$ and $\mathbf{d}_y = [1, 0, -1]$ are difference operators on vertical and horizontal directions, respectively, to approximate the gradient of image, \otimes denotes convolution (specifically 1D convolution here), γ is a balance parameter, and $\mathbf{G}_i = \left(1 + \lambda e^{-\frac{|\mathbf{d}_i \otimes \mathbf{I}|}{\sigma}}\right) \circ (\mathbf{d}_i \otimes \mathbf{I})$ is approximately the amplified gradient of \mathbf{I} . As discussed in (M. Li, Liu, Yang, Sun, & Guo, 2018b), the additional prior term $\sum_{i=x,y} \|\mathbf{d}_i \otimes \mathbf{R} - \mathbf{G}_i\|_F^2$ can reveal more structure details in the enhanced result. Since simple yet effective, we explicitly adopt such a structure revealing prior in optimization (6), which is also easy to be embedded in network, by virtue of algorithm unrolling, as shown in the following.

3.2.2 Solving Algorithm for Decomposition

Now we need to construct the algorithm for solving optimization problem (6). Jointly optimizing \mathbf{R} and \mathbf{L} is generally difficult, while if we only optimize one of them with the other fixed, the sub-problem can be relatively easier. Therefore, we adopt this alternative search strategy.

Updating \mathbf{L} : With reflectance \mathbf{R} being fixed, illumination \mathbf{L} can be updated by solving the

following optimization:

$$\min_{\mathbf{L}} \frac{1}{2} \|\mathbf{I} - \mathbf{R} \circ \mathbf{L}\|_F^2 + g_1(\mathbf{L}). \quad (7)$$

This problem can be solved by proximal gradient descent (PGD) (Parikh & Boyd, 2014) type method with the following form of iterations:

$$\mathbf{L} := \text{prox}_{\eta_1 g_1(\cdot)}(\mathbf{L} - \eta_1 d_{\mathbf{L}}), \quad (8)$$

where η_1 is the step size, $\text{prox}_{f(\cdot)}(\cdot)$ is the proximal operator depending on function $f(\cdot)$, and $d_{\mathbf{L}}$ is the descent direction related to \mathbf{L} . Though commonly chosen as gradient, $d_{\mathbf{L}}$ can indeed be any decent direction with respect to function $f_1(\mathbf{L}) = \frac{1}{2} \|\mathbf{I} - \mathbf{R} \circ \mathbf{L}\|_F^2$. Therefore, inspired by the fact that Newton method (Ypma, 1995) has better convergence than gradient descent, we adopt the following Newton descent direction (detailed calculations are provided in Appendix):

$$\begin{aligned} d_{\mathbf{L}} &= (\nabla^2 f_1(\mathbf{L}))^{-1} \nabla f_1(\mathbf{L}) \\ &= (\mathbf{R} \circ (\mathbf{R} \circ \mathbf{L} - \mathbf{I})) \oslash (\mathbf{R} \circ \mathbf{R}), \end{aligned} \quad (9)$$

where $\nabla f_1(\mathbf{L})$ and $\nabla^2 f_1(\mathbf{L})$ denote the gradient and Hessian of $f_1(\mathbf{L})$, respectively. Note that only element-wise operations are involved in Eq. (9), and thus its computational cost is with the same order as that of computing gradient.

Updating \mathbf{R} : The optimization for reflectance \mathbf{R} , by fixing illumination \mathbf{L} , can be written as

$$\min_{\mathbf{R}} \frac{1}{2} \|\mathbf{I} - \mathbf{R} \circ \mathbf{L}\|_F^2 + g_2(\mathbf{R}) + \frac{\gamma}{4} \sum_{i=x,y} \|\mathbf{d}_i \otimes \mathbf{R} - \mathbf{G}_i\|_F^2, \quad (10)$$

which can also be solved by PGD type iterations with the following form:

$$\mathbf{R} := \text{prox}_{\eta_2 g_2(\cdot)}(\mathbf{R} - \eta_2 d_{\mathbf{R}}). \quad (11)$$

Following the similar idea for updating \mathbf{L} , we try to calculate the Newton direction for descending:

$$\begin{aligned} d_{\mathbf{R}} &= (\nabla^2 f_2(\mathbf{R}))^{-1} \nabla f_2(\mathbf{R}) \\ &\approx \left((\mathbf{R} \circ \mathbf{L} - \mathbf{I}) \circ \mathbf{L} + \frac{\gamma}{2} \sum_{i=x,y} \mathbf{d}_i \otimes \mathbf{T}(\mathbf{d}_i \otimes \mathbf{R} - \mathbf{G}_i) \right) \\ &\quad \oslash (\mathbf{L} \circ \mathbf{L} + 4\gamma \mathbf{E}), \end{aligned} \quad (12)$$

Algorithm 1 Algorithm for solving optimization (6) (differences in network realization are shown in BLUE)

For $k = 1, 2, \dots, K$ Do
Update L:
1: $d_{\mathbf{L}}^{(k)} = (\mathbf{R}^{(k-1)} \circ (\mathbf{R}^{(k-1)} \circ \mathbf{L}^{(k-1)} - \mathbf{I})) \oslash (\mathbf{R}^{(k-1)} \circ \mathbf{R}^{(k-1)})$
2: $\hat{\mathbf{L}}^{(k)} = \mathbf{L}^{(k-1)} - \eta_1^{(k)} d_{\mathbf{L}}^{(k)} \Rightarrow \hat{\mathbf{L}}^{(k)} = \text{concat} \left(\mathbf{L}^{(k-1)}, \mathbf{R}^{(k-1)}, d_{\mathbf{L}}^{(k)} \right)$
3: $\mathbf{L}^{(k)} = \text{prox}_{\eta_1 g_1(\cdot)} \left(\hat{\mathbf{L}}^{(k)} \right) \Rightarrow \{\mathbf{L}^{(k)}, \mathbf{Z}_L^{(k)}\} = \text{proxNet}_{\theta_l^{(k)}} \left(\text{concat} \left(\hat{\mathbf{L}}^{(k)}, \mathbf{Z}_L^{(k-1)} \right) \right)$
Update R:
4: $\tilde{\mathbf{A}}_i^{(k)} = \mathbf{d}_i \otimes \mathbf{R}^{(k-1)} - \mathbf{G}_i, \quad i = x, y$
5: $\hat{\mathbf{A}}_i^{(k)} = \mathbf{d}_i \otimes \tilde{\mathbf{A}}_i^{(k)}, \quad i = x, y$
6: $d_{\mathbf{R}}^{(k)} = \left((\mathbf{R}^{(k-1)} \circ \mathbf{L}^{(k)} - \mathbf{I}) \circ \mathbf{L}^{(k)} + \frac{\gamma}{2} \sum_{i=x,y} \hat{\mathbf{A}}_i^{(k)} \right) \oslash (\mathbf{L}^{(k)} \circ \mathbf{L}^{(k)} + 4\gamma \mathbf{E})$
7: $\hat{\mathbf{R}}^{(k)} = \mathbf{R}^{(k-1)} - \eta_2^{(k)} d_{\mathbf{R}}^{(k)}$
8: $\mathbf{R}^{(k)} = \text{prox}_{\eta_2 g_2(\cdot)} \left(\hat{\mathbf{R}}^{(k)} \right) \Rightarrow \{\mathbf{R}^{(k)}, \mathbf{Z}_R^{(k)}\} = \text{proxNet}_{\theta_r^{(k)}} \left(\text{concat} \left(\hat{\mathbf{R}}^{(k)}, \mathbf{Z}_R^{(k)} \right) \right)$
End For

where $f_2(\mathbf{R}) = \frac{1}{2} \|\mathbf{I} - \mathbf{R} \circ \mathbf{L}\|_F^2 + g_2(\mathbf{R}) + \frac{\gamma}{4} \sum_{i=x,y} \|\mathbf{d}_i \otimes \mathbf{R} - \mathbf{G}_i\|_F^2$, \mathbf{E} is the matrix with all elements being one, \otimes^T refers to the transposed convolution, and we used the diagonal approximation to the Hessian matrix (Details are provided in Appendix).

Overall Algorithm: Putting Eqs. (8) (9) (11) (12) together, the overall updating procedure can be summarized as Algorithm 1. This algorithm can then be used to guide the design of our decomposition network.

3.2.3 Network Architecture Inspired by Algorithm Unrolling

Now we can present our network architecture for Retinex based image decomposition inspired by algorithm unrolling. It can be seen that, most of the operations are explicit, and thus can be directly transferred to network structures. The only operations not specified are the two proximal operators, which depend on the choices of $g_1(\cdot)$ and $g_2(\cdot)$. Following the idea in previous work (H. Wang et al., 2020; Xie et al., 2020), we can parameterize the proximal operators by network modules, in order to fully make use of the learning capacity of DNNs. In specific, we replace Step 3 and Step 8 in Algorithm 1 by

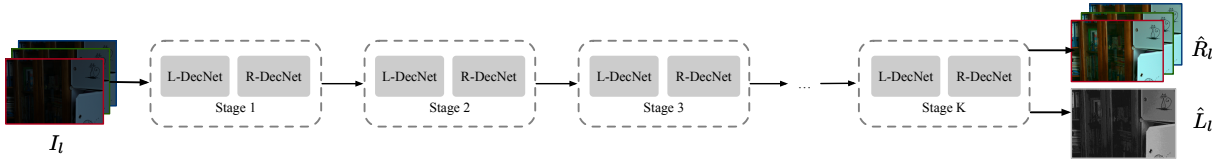
$$\mathbf{L}^{(k)} = \text{proxNet}_{\theta_l^{(k)}} \left(\hat{\mathbf{L}}^{(k)} \right), \quad (13)$$

and

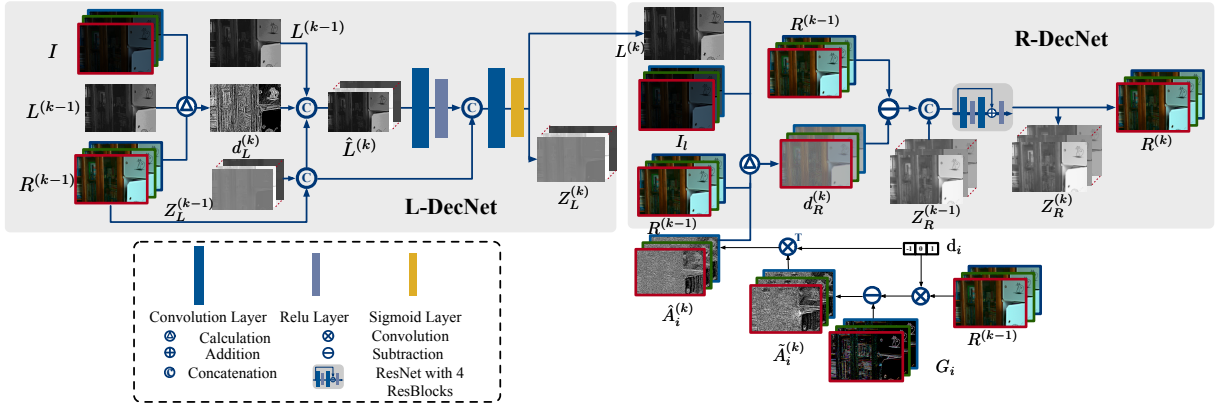
$$\mathbf{R}^{(k)} = \text{proxNet}_{\theta_r^{(k)}} \left(\hat{\mathbf{R}}^{(k)} \right), \quad (14)$$

respectively, where $\text{proxNet}_{\theta_l^{(k)}}(\cdot)$ refers to simply two convolution layers with parameters $\theta_l^{(k)}$, and $\text{proxNet}_{\theta_r^{(k)}}(\cdot)$ is composed of four ResBlocks (He, Zhang, Ren, & Sun, 2016) parameterized by $\theta_r^{(k)}$ without batch normalization. Then we can obtain two sub-networks for estimating \mathbf{L} and \mathbf{R} each stage, respectively, denoted as *L-DecNet* and *R-DecNet*, which correspond to the updating steps for \mathbf{L} and \mathbf{R} in Algorithm 1. Sequentially stacking stages containing L-DecNet and R-DecNet, the whole network for decomposition can then be constructed, which is illustrated in Fig. 2. It can be seen that, the overall decomposition network is constructed with very simple building blocks, such as convolution layers and ResBlocks.

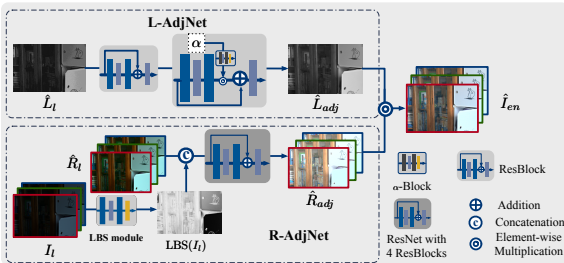
As can be observed from Fig. 2, also shown in blue in Algorithm 1, there are two architecture designs inconsistent with the solving algorithm for optimization (6). First, instead of computing $\hat{\mathbf{L}}^{(k)}$ by $\hat{\mathbf{L}}^{(k)} = \mathbf{L}^{(k-1)} - \eta_1^{(k)} d_{\mathbf{L}}^{(k)}$, we formulate $\hat{\mathbf{L}}^{(k)} = \text{concat} \left(\mathbf{L}^{(k-1)}, \mathbf{R}^{(k-1)}, d_{\mathbf{L}}^{(k)} \right)$, where $\text{concat}(\cdot)$ is the concatenation operator. Intuitively, this can provide more flexibility for $\text{proxNet}_{\theta_l^{(k)}}(\cdot)$ to integrate the information provided by last estimate $\mathbf{L}^{(k-1)}$ and descent direction $d_{\mathbf{L}}^{(k)}$ (note that $\mathbf{R}^{(k-1)}$ also appears in the calculation of $d_{\mathbf{L}}^{(k)}$), than explicitly doing so with fixed form in Line 3 of Algorithm 1. Second, auxiliary features \mathbf{Z}_L and



(a) The entire decomposition network.



(b) Design of a single stage in the decomposition network.

Fig. 2 Illustration of the proposed algorithm unrolling inspired network for Retinex decomposition.**Fig. 3** Illustration of the proposed adjustment network.

Z_R are used as input and output of proxNet for \mathbf{L} and \mathbf{R} , respectively. This is because both \mathbf{L} and \mathbf{R} are with only few channels (1 and 3, respectively), and if we exactly follow the algorithm, they will be firstly expanded to multiple channels and then fused again in each stage of the network, which means that two adjacent stages can only interact with each other through only few fused feature channels, and thus obviously lead to loss of useful information. This strategy has also been used in (H. Wang et al., 2020), though the authors did not emphasize it.

3.3 Adjustment Networks

As discussed before, due to complicated degradations, the Retinex decomposition of a low-light

image is not perfect, and thus adjustment is crucial for LIE. In this subsection, we present adjustment networks for both illumination and reflectance. The overall structures of the two networks are shown in Fig. 3.

3.3.1 Illumination Adjustment with Global Brightness

Since the illumination layer is with only one channel, and contains less information about the image, compared with the reflectance layer, we can use relatively simpler network structures. Specifically, we stack two ResBlocks to construct the adjustment network for \mathbf{L} , denoted as $L\text{-AdjNet}$. Besides, considering that the LIE problem does not have a unique and standard solution, and level of the enhancement may be decided by users, we also introduce a global brightness parameter α , similar to that in (Fan et al., 2020; Y. Zhang et al., 2021, 2019). Different from concatenating this parameter to \mathbf{L} as the input of the adjustment network considered in (Y. Zhang et al., 2021), we multiply this parameter, with a small transformation block, to the skip connection of the second ResBlock, whose effect can be more intuitively explainable. Specifically, our $L\text{-AdjNet}$ results in



Fig. 4 Enhanced image (top row) and corresponding illumination layer (bottom row) with setting $\alpha = 0, 0.3, 0.5, 0.8, 1.0$ from left to right.

the following adjusting process:

$$\mathbf{L}^{(s)} = \text{ReLU}\left(\mathbf{L}^{(s-1)} + t_s(\alpha)h_s(\mathbf{L}^{(s-1)})\right), \quad s = 1, 2, \quad (15)$$

where $t_s(\cdot)$, $s = 1, 2$ denote transformations to α , with that $t_1(\cdot) \equiv 1$ and $t_2(\cdot)$ being a small network, and $h_s(\cdot)$, $s = 1, 2$ denote the convolution layers before added to the skip connection. Therefore, the whole adjusting process can be intuitively interpreted as a two-step projected gradient descent (Boyd & Vandenberghe, 2004) for \mathbf{L} (note that the ReLU activation is intrinsically a projection operation to ensure \mathbf{L} non-negative), with the second step size controlled by α , and gradient computed by $-h_s(\cdot)$, $s = 1, 2$. We have tried to let $t_1(\cdot)$ also being a network, but the performance degenerated a little, which indicates that the first step adjustment should be sufficient enough. The influence of α is visually illustrated in Fig. 4.

The next issue is that how to determine α . In the training phase, since both the low-light and normal-light images are available, we calculate this parameter by $\alpha = \frac{1}{HW} \left\| (\tilde{\mathbf{I}}_h - \tilde{\mathbf{I}}_l) \oslash \tilde{\mathbf{I}}_h \right\|_1$, where $\tilde{\mathbf{I}}$ denotes the gray image converted from its color version \mathbf{I} , which can be interpreted as the mean relative differences of the light intensity between normal-light and low-light images. In the testing phase, if normal-light image corresponding to the input is available, this calculation is still applicable, as in our experiments on paired datasets. However, in practice, normal-light image is not available, therefore, users may vary this parameter and choose the one leading to the best visual result subjectively. For easing such manually parameter specification, we also propose a

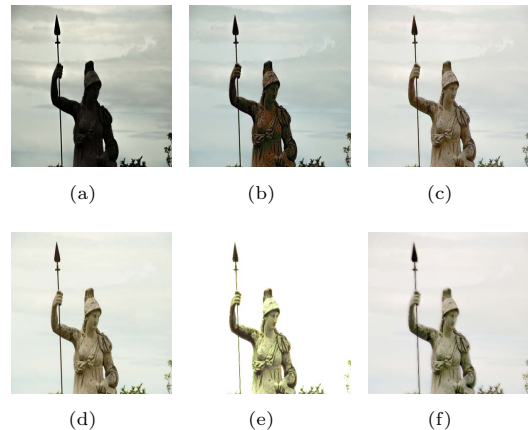


Fig. 5 (a) is the input image, and (d) is the corresponding normal-light image. (b) and (c) are the enhanced results without and with the LBS module, respectively, and (e) and (f) are the corresponding reflectance layers.

self-supervised strategy to fine-tune this parameter, as well as the whole adjustment network, detailed in Section 3.5.

3.3.2 Reflectance Adjustment with Local Brightness Sensitivity

As discussed in (Y. Zhang et al., 2021), the degradations involved in \mathbf{R} are more complicated, and information in addition to \mathbf{R} itself is important to guide adjusting \mathbf{R} . Our major observation is that, as shown in Fig. 5(a), different regions in the image have different sensitivities in brightness under the same environment, which tends to result in spatially variant degradations of \mathbf{R} . In contrast, the brightness of normal-light image, as shown in Fig. 5(d), is more spatially homogeneous. Therefore, the pixel-wise brightness difference between low-light and normal-light images can be a useful feature for adjusting \mathbf{R} . However, since the

groundtruth normal-light image is unavailable at test time, we try to predict such information by the low-light image. Specifically, we design a simple local brightness sensitivity (LBS) module with a two-layer convolution structure to achieve this goal. During training, the target output of LBS module is defined as $(\tilde{\mathbf{I}}_h - \tilde{\mathbf{I}}_l) \oslash \tilde{\mathbf{I}}_h$, where $\tilde{\mathbf{I}}$ denotes the gray image converted from its color version \mathbf{I} . This target can be roughly regarded as the relative brightness difference between low-light and normal-light images. The extracted LBS feature is then concatenated with \mathbf{R} , as the input of a ResNet with 4 ResBlocks for final adjustment. As can be seen from Fig. 5, with this LBS feature extraction module, the obtained reflectance is with more details, which leads to better enhancement result, well addressing the non-uniform brightness issue.

3.4 Loss Functions and Network Training

3.4.1 Loss Function for Decomposition Network

The training of decomposition network is not easy, since only image pairs of \mathbf{I}_h and \mathbf{I}_l are available, while neither of them have groundtruth reflectance and illumination. Therefore, following the idea from (Y. Zhang et al., 2021), we resort to several properties by Retinex model: consistency in reflectance between low-light and normal-light images, smoothness in illumination and reconstruction by decomposition. Specifically, denoting $(\mathbf{I}_l, \mathbf{I}_h)$ as the training pair of low-light image and corresponding normal-light one, and $(\mathbf{R}_l^{(k)}, \mathbf{L}_l^{(k)})$ and $(\mathbf{R}_h^{(k)}, \mathbf{L}_h^{(k)})$ the Retinex decomposition for low-light and normal-light images, respectively, at the k th stage, there are three terms included in our loss function:

- $\mathcal{L}_R^{(k)} = \frac{1}{HW} \left\| \mathbf{R}_l^{(k)} - \mathbf{R}_h^{(k)} \right\|_F^2$, which measures the closeness between the reflectance layers obtained from low-light and normal-light images, respectively;

- $\mathcal{L}_L^{(k)} = \frac{1}{HW} \left(\left\| \frac{\nabla \mathbf{L}_l^{(k)}}{\max(|\nabla \mathbf{I}_l|, \epsilon)} \right\|_1 + \left\| \frac{\nabla \mathbf{L}_h^{(k)}}{\max(|\nabla \mathbf{I}_l|, \epsilon)} \right\|_1 \right)^2$, which is computed in the gradient domain in order to enforce smoothness to the illumination layers;
- $\mathcal{L}_{\text{rec}}^{(k)} = \frac{1}{HW} \left(\left\| \mathbf{I}_l - \mathbf{R}_l^{(k)} \circ \mathbf{L}_l^{(k)} \right\|_F^2 + \left\| \mathbf{I}_h - \mathbf{R}_h^{(k)} \circ \mathbf{L}_h^{(k)} \right\|_F^2 \right)$, which tries to reconstruct the images by decomposed reflectance and illumination according to Retinex model.

Combining these terms together, the overall loss is then defined as

$$\mathcal{L}_{\text{dec}} = \gamma_R \sum_{k=1}^K \mathcal{L}_R^{(k)} + \gamma_L \sum_{k=1}^K \mathcal{L}_L^{(k)} + \gamma_{\text{rec}} \sum_{k=1}^K \mathcal{L}_{\text{rec}}^{(k)}, \quad (16)$$

where γ_R , γ_L and γ_{rec} are the balance parameters, and set to 0.1, 1 and 1000, respectively, in our experiments. Note that, since our estimation for reflectance and illumination is realized stage-wise in a progressive way, we can place loss at each stage instead of only penalize the final output, by virtue of the algorithm unrolling methodology.

3.4.2 Loss Function for Adjustment Networks

For the adjustment networks, there are also several components to be considered in loss function. Specifically, the adjustment results $\hat{\mathbf{R}}_{\text{adj}}$ and $\hat{\mathbf{L}}_{\text{adj}}$ for both reflectance and illumination should be supervised, as well as the final enhanced image. In addition, as mentioned in Section 3.3.2, the LBS module should also be supervised. We then discuss the loss term for each of them.

For $\hat{\mathbf{R}}_{\text{adj}}$ and $\hat{\mathbf{L}}_{\text{adj}}$, considering that ideally the Retinex decomposition to the normal-light image can be treated as groundtruth, we can input the normal-light image to the decomposition network and use the output, with stop-gradient operation, as the pseudo groundtruth to supervise $\hat{\mathbf{R}}_{\text{adj}}$ and $\hat{\mathbf{L}}_{\text{adj}}$. Specifically, denoting $(\mathbf{R}_h^{(K)}, \mathbf{L}_h^{(K)})$ the output of the decomposition network by inputting

²Here, ∇ stands for the first order difference operator containing both horizontal and vertical directions, i.e., $\nabla \mathbf{I} = [\mathbf{d}_x \otimes \mathbf{I}, \mathbf{d}_y \otimes \mathbf{I}]$ using the notation in Eq. (6).

normal-light image \mathbf{I}_h , we define

$$\mathcal{L}_{R_{\text{adj}}} = 1 - \text{SSIM} \left(\hat{\mathbf{R}}_{\text{adj}}, \text{StopGradient} \left(\mathbf{R}_h^{(K)} \right) \right), \quad (17)$$

and

$$\mathcal{L}_{L_{\text{adj}}} = \frac{1}{HW} \left\| \hat{\mathbf{L}}_{\text{adj}} - \text{StopGradient} \left(\mathbf{L}_h^{(K)} \right) \right\|_F^2, \quad (18)$$

respectively, where $\text{StopGradient}(\cdot)$ denotes the stop-gradient operation, and $\text{SSIM}(\cdot, \cdot)$ is structural similarity (SSIM) (Z. Wang, Bovik, Sheikh, & Simoncelli, 2004) between two images. Similarly, for the LBS module, we also simply measure the closeness between output and target by

$$\mathcal{L}_{\text{lbs}} = \frac{1}{HW} \left\| \text{LBS}(\mathbf{I}_l) - (\tilde{\mathbf{I}}_h - \tilde{\mathbf{I}}_l) \oslash \tilde{\mathbf{I}}_h \right\|_F^2. \quad (19)$$

Since the groundtruth normal-light image \mathbf{I}_h is available in the training phase, the final enhanced image $\hat{\mathbf{I}}_{\text{en}} = \hat{\mathbf{R}}_{\text{adj}} \circ \hat{\mathbf{L}}_{\text{adj}}$ can be easily supervised by minimizing the closeness between them. In addition to the commonly used mean squared error (MSE) loss, we also adopt the perceptual loss (Johnson, Alahi, & Fei-Fei, 2016; Ledig et al., 2017) and color loss (R. Wang et al., 2019) (the second and third term below), and the overall loss is

$$\begin{aligned} \mathcal{L}_{\text{en}} = & \frac{1}{HW} \left\| \hat{\mathbf{I}}_{\text{en}} - \mathbf{I}_h \right\|_F^2 \\ & + \frac{1}{HW} \left\| \phi_{\text{vgg}}(\hat{\mathbf{I}}_{\text{en}}) - \phi_{\text{vgg}}(\mathbf{I}_h) \right\|_F^2, \quad (20) \\ & + \frac{1}{HW} \sum_p \angle((\hat{\mathbf{I}}_{\text{en}})_p, (\mathbf{I}_h)_p) \end{aligned}$$

where $\phi_{\text{vgg}}(\cdot)$ is a pre-trained VGG-Net (Simonyan & Zisserman, 2014), $\angle(\cdot, \cdot)$ denotes the angle between two RGB vectors, and p indicates the position of an image pixel. We will show in Section 4.3 that each term in Eq. (20) facilitate to a promising performance.

Putting all of above loss terms together, the final loss function for adjustment networks is defined as

$$\mathcal{L}_{\text{adj}} = \eta_L \mathcal{L}_{L_{\text{adj}}} + \eta_R \mathcal{L}_{R_{\text{adj}}} + \eta_{\text{lbs}} \mathcal{L}_{\text{lbs}} + \eta_{\text{en}} \mathcal{L}_{\text{en}}, \quad (21)$$

where the balance parameters η_L , η_R , η_{lbs} and η_{en} are set to 0.05, 0.05, 0.1 and 20, respectively.

3.4.3 Training Strategy

Our whole framework, including both decomposition and adjustment networks, is trained in an end-to-end fashion. However, considering that decomposition network and adjustment network play different roles in the LIE task, we use two optimizers for these two parts (detailed in Section 4.1.4), respectively.

As for the training data, we use a simple yet effective data augmentation technique. Specifically, note that the normal-light image itself can be seen as a special case of light-light image, except that the light condition is normal. Therefore, we add image pairs in the form of $(\mathbf{I}_h, \mathbf{I}_h)$, in addition to $(\mathbf{I}_l, \mathbf{I}_h)$, to the training set. In this sense, the range of light conditions of low-light image in the dataset can be enlarged.

3.5 Self-supervised Fine-tuning at Test Time

As discussed in Section 3.3.1, there is a global brightness parameter α to be specified manually in applying our network to real low-light images. Therefore, we present a self-supervised fine-tuning strategy to avoid such manual specification at test time. It should be mentioned that this fine-tuning strategy can not only be used to tune α , but indeed also be used to fine-tune a part of the whole network. To our knowledge, the test time training (fine-tuning) can be dated back to (Y. Sun et al., 2020), and similar methodology has been used in image dehazing problem (Chen, Wang, Yang, & Liu, 2021).

The core idea of our fine-tuning strategy is to first synthesize a pseudo normal-light image $\hat{\mathbf{I}}_{\text{syn}}$ from the low-light image itself, and then update the network by minimizing the following loss function:

$$\mathcal{L}_{\text{ft}} = \frac{1}{HW} \left\| \hat{\mathbf{I}}_{\text{ft}} - \hat{\mathbf{I}}_{\text{syn}} \right\|_F^2, \quad (22)$$

where $\hat{\mathbf{I}}_{\text{ft}}$ denotes the enhanced image by the fine-tuned network. Here, the synthesized normal-light image needs not necessarily to be perfect, while it is enough to only provide some useful information as guidance for fine-tuning, such as brightness and contrast. Therefore, traditional image processing tools, that have been used in existing LIE methods, can be adopted to synthesize the normal-light



Fig. 6 Visual comparison of the enhanced images with and without the self-supervised fine-tuning strategy, together with the synthesized guiding image.

image. Specifically, we first directly increase the global brightness of the low-light image, and then use CLAHE (Zuiderveld, 1994) to enhance the local contrast, followed by BM3D (Dabov, Foi, Katkovnik, & Egiazarian, 2007) to suppress noise. Using the synthesized image and loss function, we can then fine-tune the adjustment networks, i.e., L-AdjNet and R-AdjNet, together with parameter α , with about 30 iterations. The reason why we only fine-tune the adjustment networks instead of the whole architecture is two-fold. First, after training, the decomposition network is already powerful enough for the task we concerning. Second, due to the learning capacity of DNN, the network could overfit to the synthesized image, especially considering that the decomposition network has much more parameters.

Fig. 6 demonstrate the effectiveness of the proposed self-supervised fine-tuning strategy. As can be seen, though the quality of $\hat{\mathbf{I}}_{\text{syn}}$ is not satisfactory, it provides useful information for fine-tuning, especially the color and contrast information. Therefore, the fine-tuned image looks slightly better than the direct output of the network.

It should also be mentioned that, though effective, the test time fine-tuning could be costly regarding the inference time, and thus there is a balance between performance and time that should be taken into consideration in practice.

4 Experiments

In this section, we present experimental results to demonstrate the effectiveness of the proposed method. We first briefly introduce the experimental settings, including datasets, competing methods, performance metrics and some implementation details. Then we present both the quantitative and visual results of our method, in comparison with existing methods. In addition,

ablation studies are also provided to more comprehensively analyze the proposed framework. In the following, our method is referred to as RAUNA, which is short for “Retinex based Algorithm UNrolling and Adjustment”, and an additional subscript “ft” indicates the proposed fine-tuning strategy.

4.1 Experimental Settings

4.1.1 Datasets

We adopt four popular datasets for the LIE problem in our experiments, including LOL (Wei et al., 2018), MIT-Adobe FiveK (Bychkovsky, Paris, Chan, & Durand, 2011), NPE (S. Wang et al., 2013b) and DICM (Lee, Lee, & Kim, 2013). Among these datasets, LOL and MIT-Adobe FiveK are composed of low/normal light image pairs, while the rest are with only low-light images. It should also be mentioned that, though both are with low/normal light image pairs, the characteristics of LOL and MIT-Adobe FiveK datasets are very different due to the collection ways. Specifically, image pairs in LOL dataset are collected by varying exposure time and ISO at the same scene, and thus the low-light images are with complex noise and contrast bias. In contrast, for MIT-Adobe FiveK dataset, only the low-light images are real-captured without noise, while the corresponding normal-light images are obtained by expert retouching. We use the default training/testing split for LOL dataset, while follow the split used in (R. Wang et al., 2019; Y. Zhang et al., 2021) for MIT-Adobe FiveK. Summary of used datasets is provided in Table 1.

4.1.2 Competing Methods

For competing methods, we consider both traditional and deep-learning based methods for a comprehensive comparison. In specific, we adopt four representative traditional methods, including

Table 1 Summary of used datasets in experiments.

Dataset	Size (Train/Test)	Paired	Type
LOL (Wei et al., 2018)	485/15	Yes	Real
MIT-Adobe FiveK (Bychkovsky et al., 2011)	4500/500	Yes	Synthesized
NPE (S. Wang et al., 2013b)	84	No	Real
DICM (Lee et al., 2013)	64	No	Real

CLAHE (Zuiderveld, 1994), CLAHE with BM3D, LR3M (Ren et al., 2020) and NPE (S. Wang et al., 2013b). As for deep learning based methods, we adopt recently proposed state-of-the-art ones, including Zero-DCE++ (C. Li et al., 2021), KinD++ (Y. Zhang et al., 2021), CSD-Net (Ma et al., 2021), DeepUPE (R. Wang et al., 2019), MBLLEN (Lv et al., 2018), RetinexNet (Wei et al., 2018), RUAS (R. Liu et al., 2021), TBEFN (Lu & Zhang, 2020), SGM (W. Yang et al., 2021), DRBN (W. Yang et al., 2020) and KinD++ (Y. Zhang et al., 2021). Among the deep learning based methods, CSDNet, RetinexNet, MBLLEN, TBEFN, SGM, KinD++ and RUAS are fully supervised, Zero-DCE++ is unsupervised, and DRBN is semi-supervised (using additional unpaired data).

4.1.3 Evaluation Metrics

We adopt in total five metrics, including PSNR, SSIM (Z. Wang et al., 2004), NIQE (Mittal, Soundararajan, & Bovik, 2013), LOE (S. Wang et al., 2013b) and LOE_{ref} (Y. Zhang et al., 2021), to comprehensively assess the performance of all competing methods. Among them, PSNR and SSIM are two commonly used metrics for image quality assessment (IQA) with reference image, while NIQE is a general IQA measurement without reference. LOE is a metric specifically designed for evaluating the performance of LIE methods. However, it was original defined in a blind way, that the reference image to compute this metric is chosen as the input low-light image (S. Wang et al., 2013b), which is more or less problematic as pointed in (X. Guo, 2016). Therefore, LOE can be reasonable modified to LOE_{ref} by replacing the low-light image by its corresponding normal-light one as the reference (Y. Zhang et al., 2021), when groundtruth is available. Another thing should be mentioned that all the metrics in our experiments are evaluated with RGB channels.

4.1.4 Implementation Details

All experiments are conducted on a computer with Intel i7 3.40GHz (CPU), NVIDIA RTX3080 (GPU) and Ubuntu 18.04 LTS (OS). Our method is implemented using PyTorch 1.7.0, while other methods are implemented according to their codes. We initialize our model parameters following (He et al., 2016), and ADAM (Kingma & Ba, 2015) is used for optimization. The initial learning rates are set to 1×10^{-5} and 1×10^{-3} for decomposition and adjustment networks, respectively, and then is divided by 10 at the 2nd and 3rd epochs for decomposition network, while at the 60th epoch for adjustment network. The model is trained with 70 epochs in total. Since LOL and MIT-Adobe FiveK datasets contain both training and testing sets, we can train and test our model on corresponding ones. For NPE and DICM datasets, since no groundtruth is provided, we directly test using our model trained on LOL. During training, we use cropped image patches in each training batch. Specifically, for LOL dataset, 8 pairs of patches with size 64×64 are used in each batch, and for MIT-Adobe FiveK dataset, 16 pairs of patches with size 48×48 are used. Since LOL dataset is more challenging than MIT-Adobe FiveK dataset, we use a 17-stage decomposition network for LOL, while 13-stage for MIT-Adobe FiveK.

4.2 Comparison with Existing Methods

4.2.1 Results on LOL Dataset

The quantitative and visual results of all competing methods on LOL dataset are shown in Table 2 and Fig. 7. Following (W. Yang et al., 2020), we also report the results after GC to emphasize detail fidelity of the enhanced images in evaluation, except for KinD++ and our methods since the adjustment networks within their frameworks can automatically adjust the global illumination,

Table 2 Quantitative comparison of all competing methods on LOL dataset. The best and second best results, with respect to each IQA metric, are highlighted in **RED** and **BLUE**, respectively.

Method	Without GC					With GC				
	SSIM \uparrow	PSNR \uparrow	NIQE \downarrow	LOE _{ref} \downarrow	LOE \downarrow	SSIM \uparrow	PSNR \uparrow	NIQE \downarrow	LOE _{ref} \downarrow	LOE \downarrow
CLAHE (Zuiderveld, 1994)	0.494	14.36	9.032	808.6	787.1	0.772	17.77	7.789	358.1	285.9
CLAHE+BM3D	0.702	15.65	5.731	767.7	749.5	0.836	18.21	6.024	350.4	284.7
LR3M (Ren et al., 2020)	0.440	10.31	7.540	290.9	332.1	0.707	15.77	6.628	298.6	348.4
NPE (S. Wang et al., 2013b)	0.697	17.14	8.439	463.6	422.7	0.709	17.78	8.371	468.9	430.8
Zero-DCE++ (C. Li et al., 2021)	0.718	15.42	7.896	257.3	195.1	0.768	18.08	7.793	260.4	210.4
CSDNet (Ma et al., 2021)	0.870	20.75	4.023	373.9	341.0	0.873	22.55	4.018	374.0	339.5
DeepUPE (R. Wang et al., 2019)	0.549	12.80	7.524	369.6	297.3	0.772	18.43	7.863	359.0	305.4
MBLLEN (Lv et al., 2018)	0.788	17.91	3.584	362.2	383.7	0.789	18.29	3.544	369.3	394.2
RetinexNet (Wei et al., 2018)	0.648	16.98	8.878	462.0	486.2	0.646	16.96	8.799	466.0	490.1
RUAS (R. Liu et al., 2021)	0.666	16.50	6.340	220.0	125.6	0.742	17.03	6.258	215.5	133.4
TBEFN (Lu & Zhang, 2020)	0.831	17.43	3.437	325.7	342.8	0.836	17.74	3.418	327.4	345.6
SGM (W. Yang et al., 2021)	0.782	16.90	4.613	428.8	411.2	0.771	16.46	4.627	429.1	410.2
DRBN (W. Yang et al., 2020)	0.853	18.67	5.110	488.1	501.2	0.853	19.13	5.449	487.9	501.9
KinD++ (Y. Zhang et al., 2021)	0.863	19.82	5.111	254.2	207.9	-	-	-	-	-
RAUNA	0.874	22.82	4.213	189.2	126.5	-	-	-	-	-
RAUNA _{ft}	0.887	24.58	4.120	196.5	126.5	-	-	-	-	-

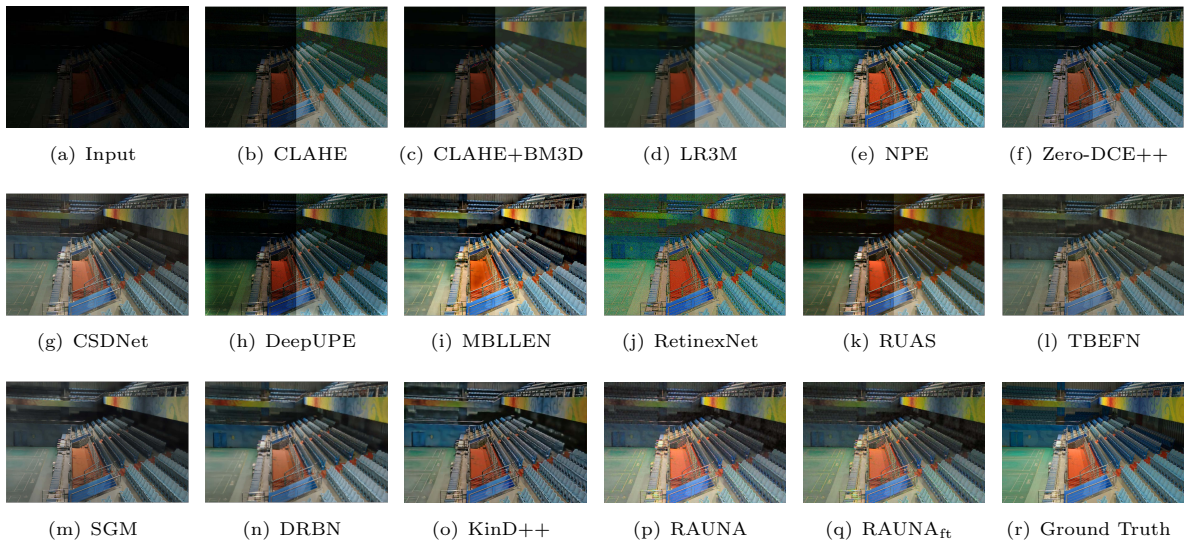


Fig. 7 Visual results of competing methods on LOL dataset. For (b)-(n), the left and parts are from enhanced images without and with Gamma Correction, respectively.

with reference to groundtruth normal-light image or pseudo one.

It can be seen from Table 2, our methods achieve the best performance under all metrics that computed with reference to groundtruth normal-light images, including both the general IQA metrics, i.e., PSNR and SSIM, and that specifically for LIE problem, i.e., LOE_{ref}. Besides, for blind IQA metrics, our methods are also very competitive. The better performance of the proposed methods can be more directly observed from Fig. 7. Specifically, most of the competing methods do not perform very well on this challenging image, that their results could still contain unexpected degradations, such as low brightness, color bias and noise, while the results by CSDNet,

KinD++ and our methods are relatively more acceptable. However, the result by CSDNet seems more noisy and with less contrast, and KinD++ over-smooths some regions of the image. In comparison with other methods, our methods can produce relatively more balanced results regarding brightness, contrast, color bias and noise.

4.2.2 Results on MIT-Abobe FiveK Dataset

As mentioned before, images in MIT-Abobe FiveK dataset are collected and synthesized without noise, and thus it is relatively easier for a method to perform well. Similar as before, we report the both results with and without GC, except for KinD++ and our methods. The quantitative and

Table 3 Quantitative comparison of all competing methods on MIT-Adobe FiveK dataset. The best and second best results are highlighted in **RED** and **BLUE**, respectively.

Method	Without GC					With GC				
	SSIM \uparrow	PSNR \uparrow	NIQE \downarrow	LOE _{ref} \downarrow	LOE \downarrow	SSIM \uparrow	PSNR \uparrow	NIQE \downarrow	LOE _{ref} \downarrow	LOE \downarrow
CLAHE (Zuiderveld, 1994)	0.543	14.06	4.391	965.1	966.8	0.847	19.00	3.731	360.8	347.2
CLAHE+BM3D	0.620	14.06	5.627	958.8	960.5	0.798	18.84	5.186	360.2	346.5
LR3M (Ren et al., 2020)	0.708	15.99	5.275	273.0	283.8	0.737	18.19	5.258	272.0	283.6
NPE (S. Wang et al., 2013b)	0.795	17.50	3.735	454.1	473.4	0.804	18.10	3.743	452.1	470.4
Zero-DCE++ (C. Li et al., 2021)	0.766	15.65	3.694	311.0	370.6	0.810	17.49	3.708	309.2	326.9
CSDNet (Ma et al., 2021)	0.866	19.97	3.794	298.0	316.4	0.904	22.90	3.815	297.6	311.6
DeepUPE (R. Wang et al., 2019)	0.872	19.71	3.817	801.5	372.8	0.879	20.60	3.833	370.3	372.4
MBLLEN (Lv et al., 2018)	0.815	19.61	3.851	74.5	67.4	0.837	20.81	3.740	77.5	84.1
RetinexNet (Wei et al., 2018)	0.687	12.59	4.475	1333.0	1369.3	0.699	13.87	4.586	1330.7	1366.3
RUAS (R. Liu et al., 2021)	0.836	18.33	3.927	164.9	154.9	0.854	19.58	3.969	168.5	154.2
TBEFN (Lu & Zhang, 2020)	0.752	14.77	3.799	492.7	514.8	0.792	16.81	3.762	490.2	510.8
SGM (W. Yang et al., 2021)	0.773	16.29	3.724	614.3	679.2	0.785	16.87	3.725	614.0	632.3
DRBN (W. Yang et al., 2020)	0.674	16.21	5.438	708.7	711.6	0.775	18.27	5.444	708.4	711.8
KinD++ (Y. Zhang et al., 2021)	0.850	22.64	4.151	143.3	142.5	-	-	-	-	-
RAUNA	0.901	23.52	3.691	97.8	98.1	-	-	-	-	-
RAUNA _{ft}	0.910	25.43	3.677	92.0	95.8	-	-	-	-	-

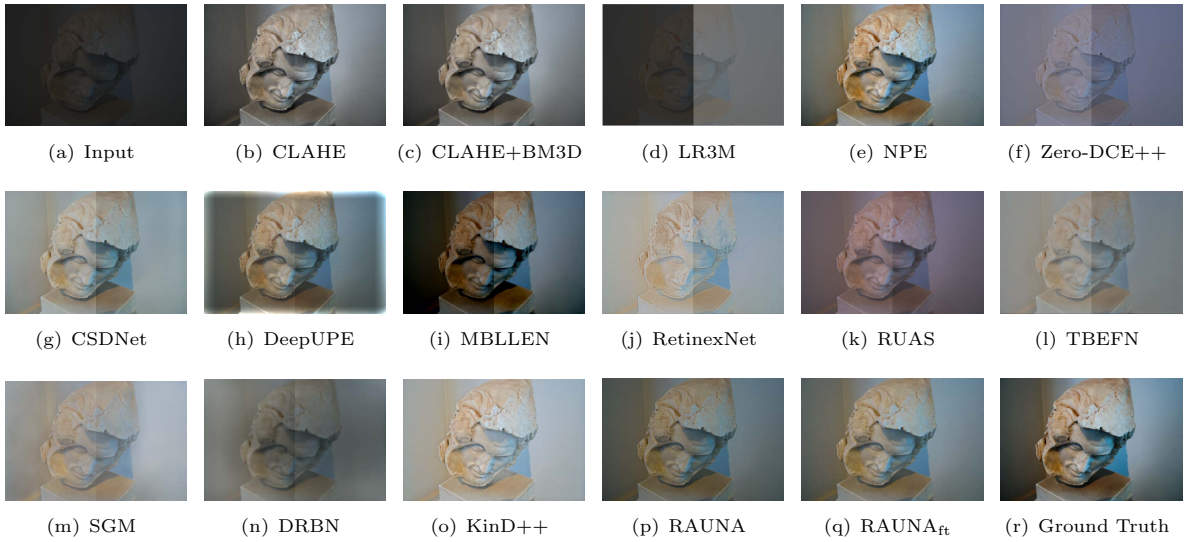


Fig. 8 Visual results of competing methods on MIT-Adobe FiveK dataset. For (b)-(n), the left and parts are from enhanced images without and with Gamma Correction, respectively.

visual results of all competing methods are shown in Table 3 and Fig. 8.

As can be seen from Table 3, the proposed methods again achieve the best performance in most of the adopted IQA metrics, while perform the second best in the LOE metrics. However, as show in Fig. 8, the visual result of MBLLEN, that achieves the best performance regarding LOEs, is still not very satisfactory, especially for the brightness. Also, the visual results of almost all methods shown in Fig. 8 are better than those on LOL dataset, which is due to the fact that the dataset is less noisy as mentioned before. These results further substantiate the effectiveness of our LIE framework.

4.2.3 Results on Unpaired Datasets

Since there are no groundtruth normal-light images available on the unpaired NPE and DICM datasets, we adopt the blind IQA metrics, i.e., NIQE and LOE, and summarize the results in Table 4. As can be seen from the table, our methods have the best performance with respect to the LIE-oriented LOE metric, showing its promising ability in this task. As for the NIQE metric, which is for general purpose IQA, though not the best, our methods still perform very competitively.

The better performance of our methods can be more directly observed from the visual results shown in Figs. 9 and 10. Specifically, our methods

Table 4 Quantitative comparison of all competing methods on NPE and DICM Datasets. The best and second best results are highlighted in **RED** and **BLUE**, respectively.

Method	DICM		NPE	
	NIQE ↓	LOE ↓	NIQE ↓	LOE ↓
CLAHE (Zuiderveld, 1994)	3.659	237.1	3.093	337.2
CLAHE+BM3D	5.481	241.0	4.140	338.6
LR3M (Ren et al., 2020)	4.963	283.4	4.377	295.3
NPE (S. Wang et al., 2013b)	3.669	320.6	3.030	366.6
Zero-DCE++ (C. Li et al., 2021)	3.589	189.1	3.211	227.9
CSDNet (Ma et al., 2021)	3.697	312.3	3.287	344.1
DeepUPE (R. Wang et al., 2019)	3.687	245.2	3.440	299.4
MBLLEN (Lv et al., 2018)	3.841	266.0	4.165	228.2
RetinexNet (Wei et al., 2018)	5.003	504.9	4.151	1478.5
RUAS (R. Liu et al., 2021)	4.055	213.8	4.918	361.5
TBEFN (Lu & Zhang, 2020)	2.903	351.4	3.062	376.4
SGM (W. Yang et al., 2021)	3.083	411.8	3.079	510.9
DRBN (W. Yang et al., 2020)	4.739	642.3	4.583	660.1
KinD++ (Y. Zhang et al., 2021)	3.173	371.0	3.406	455.9
RAUNA	3.155	188.7	3.153	227.2
RAUNA _{ft}	3.124	188.4	3.238	224.9

can not only better adjust the global brightness, but also successfully deal with the non-homogeneous light conditions. For example, the input image in Fig. 10 has a bright region in the tower, while a dark region in the building, and most of the competing methods either fail to brighten the darker region, or over-enhance the brighter region. In comparison, our methods can properly tune the brightness of the darker region, while avoid overexposure in the brighter region. Besides, the results of our methods are with less color bias, compared with another two competitive methods, Zero-DCE++ and KinD++.

4.2.4 Model and Inference Complexity

For deep learning methods, there is always a trade-off between performance and complexity (model and inference), which is important for practical applications. Therefore, we also compare the model and inference complexities of deep learning based methods, including ours. Specifically, we first summarize the statistics regarding complexity on LOL dataset in Table 5, and these statistics show that, though not the best, both the model and inference complexities of our method are not too high. Then we plot in Fig. 11 the performance with respect to PSNR on LOL dataset, versus the statistics from Table 5. It can be seen that our method performs the best with relatively low

inference time, and the model size is also not too large, which indicates that our method achieves a promising trade-off between performance and complexity.

4.3 Ablation Study

In this Section, we conduct experiments to verify the necessity of each component in our framework, including network architectures, loss functions and data augmentation. The overall results on LOL dataset are summarized in Table 6 and visualized in Fig. 12. The details are provided in the following.

4.3.1 Ablation on Model Components

We first demonstrate the necessity of the algorithm unrolling design for the decomposition network. Specifically, since the main building blocks in our decomposition network is ResBlocks in R-DecNet and convolution layers in L-DecNet, we construct a network by keeping such structures while ignoring other operations led by algorithm unrolling. It is easy to see that this newly constructed network is with the similar complexity as that of the original decomposition network. We then use this network in our framework to see its performance. It can be seen from Table 6 that

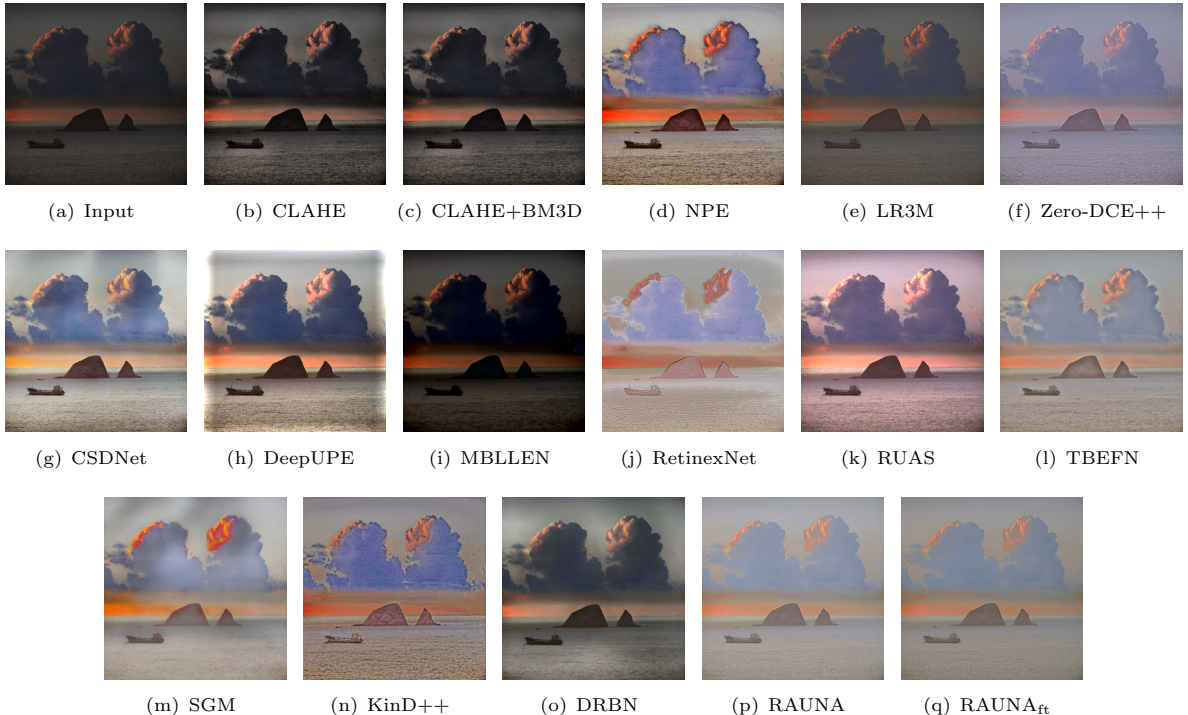


Fig. 9 Visual results of competing methods on NPE dataset.

Table 5 Comparison of model and inference complexities of deep learning based LIE methods.

Method	Test Time/s	Size/M	FLOPs/G	Platform
Zero-DCE++ (C. Li et al., 2021)	0.002	0.011	2.535	PyTorch
CSDNet (Ma et al., 2021)	0.012	17.272	121.888	PyTorch
DeepUPE (R. Wang et al., 2019)	0.032	0.594	0.059	PyTorch
MBLLEN (Lv et al., 2018)	2.981	0.450	192.923	TensorFlow
RetinexNet (Wei et al., 2018)	0.841	0.555	135.997	TensorFlow
RUAS (R. Liu et al., 2021)	0.023	0.003	0.870	PyTorch
TBEFN (Lu & Zhang, 2020)	0.399	0.145	24.112	TensorFlow
SGM (W. Yang et al., 2021)	0.120	2.308	193.103	PyTorch
DRBN (W. Yang et al., 2020)	1.210	0.577	42.865	PyTorch
KinD++ (Y. Zhang et al., 2021)	9.013	8.275	2710.247	TensorFlow
RAUNA	0.095	1.850	413.303	PyTorch

the performance significantly drops, which demonstrates the importance of algorithm unrolling. Visual results in Fig. 12 also clearly substantiate this observation. We then diagnose the effect of the number of stages in the decomposition network, and the results are shown in Table 7. As can be seen, with relatively more stages, the performance can be improved. However, if too many stages were used, the performance could drop, which could be due to overfitting issue.

Then we justify the role of the explicit structure-revealing prior, i.e., the last term in Eq. (6), in the whole network, as using this term is one of the major differences between our method and existing algorithm unrolling inspired methods for LIE. Specifically, we can remove all the operations related to this prior, and see the performance of the resulted network. It is seen from Table 6 that without this explicit prior, the performance also drops a lot, which indicates that it provides

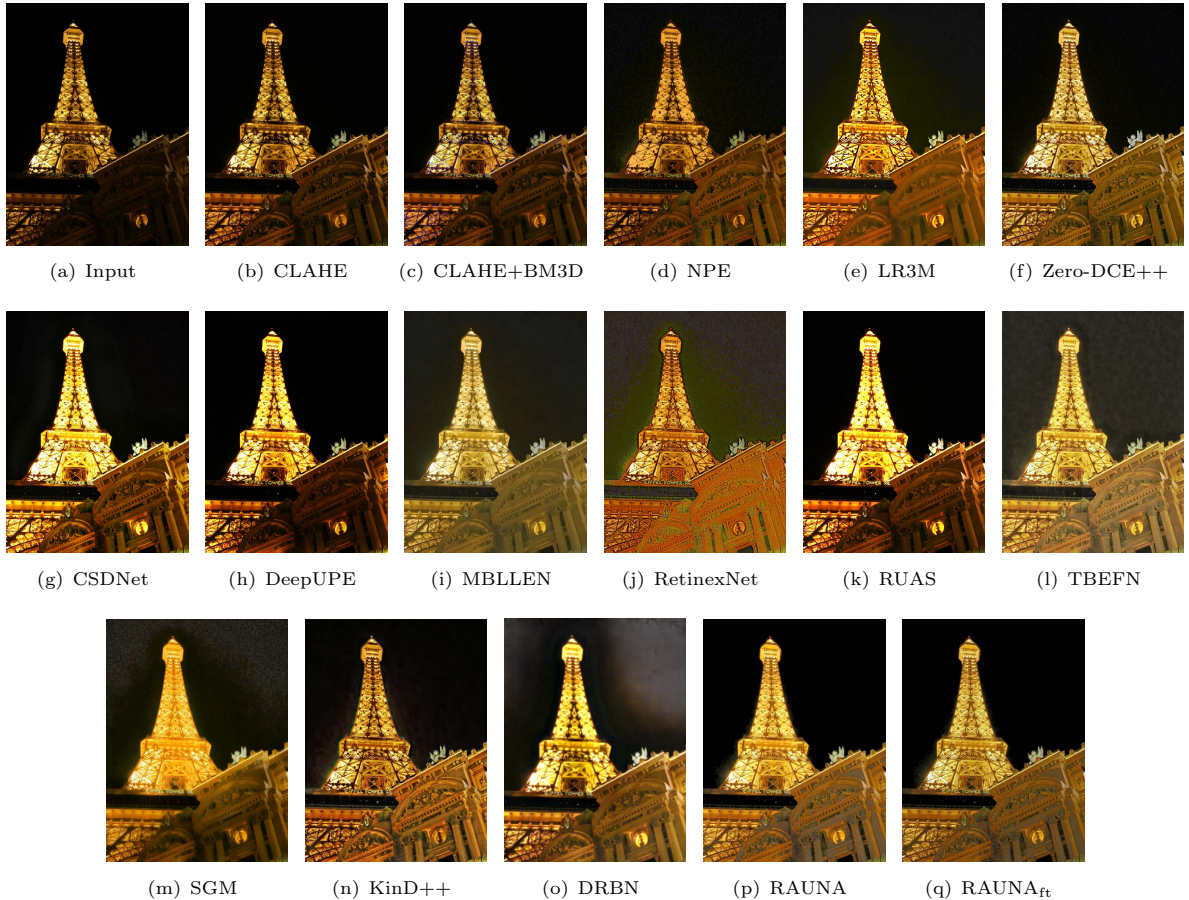


Fig. 10 Visual results of competing methods on DICM dataset.

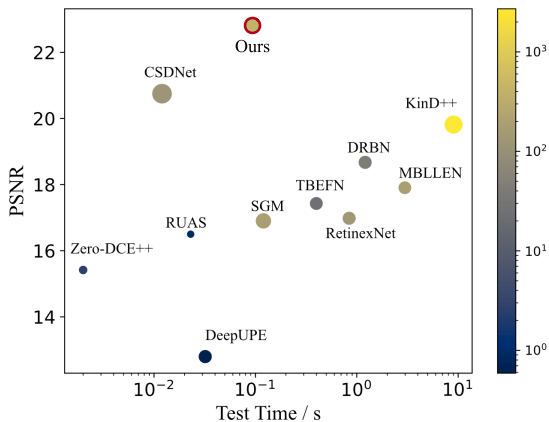


Fig. 11 Visualization of model and inference complexities of deep learning based methods. The horizontal axis refers to number of parameters. The vertical axis refers to PSNR value. The size of the circles refers to the test time, that the smaller circle indicates a shorter time. The color refers to value of FLOPs.

an effective hint for the LIE problem, especially in contrast as can be observed from Fig. 12. Since there is a tuning parameter γ in this prior term, we also visualize its influence to the enhancement result in Fig. 13. As can be seen from the figure, the saturation is approximately in proportion to γ . In our experiments, we set $\gamma = 0.1$ for promising performance.

Next we quantify the effect of the LBS module, as we have already visually demonstrated its effectiveness in Fig. 5. The result in Table 6 shows that this LBS module, though very simple, is very important to the final performance.

4.3.2 Ablation on Loss Function

In Section 3.4, we have introduced several loss terms in order to train the network. For most modules, we only place one loss term each, while the exception is the final reconstruction loss \mathcal{L}_{en}

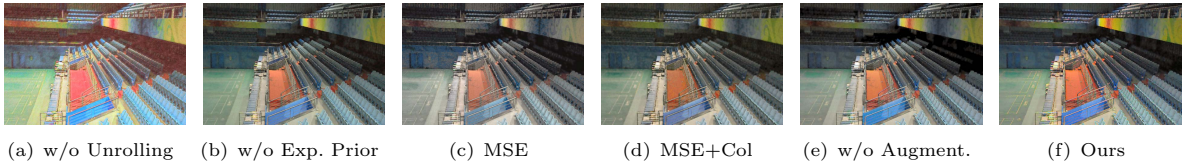


Fig. 12 Visual comparison of ablation experiments.

Table 6 Quantitative results of ablation experiments.

Setting		SSIM \uparrow	PSNR \uparrow
Model	w/o Unrolling	0.771	19.37
	w/o Explicit Prior	0.870	22.19
	w/o LBS	0.767	19.91
Loss	MSE	0.839	22.02
	MSE+Color	0.848	21.94
Data	w/o Augmentation	0.860	22.39
Ours		0.874	22.82

Table 7 Quantitative results on LOL dataset, with respect to the number of stages within the decomposition network.

Stage	5	10	12	15	17	20
SSIM \uparrow	0.850	0.851	0.852	0.851	0.874	0.855
PSNR \uparrow	20.53	21.15	21.65	21.69	22.82	20.57

containing three terms, i.e., MSE, perceptual and color losses. Therefore, we conduct ablation experiments by removing one or two terms, and the results on LOL dataset are shown in Table 6. As can be seen, all of the three terms can benefit to the final performance. Although there seems to be a trade-off in using color loss, regarding IQA metrics, the visual results in Fig. 12 show that the color bias can be alleviated by introducing color loss in addition to pure MSE loss.

4.3.3 Ablation on Data Augmentation

In Section 3.4.3, we have discussed a simple data augmentation strategy for training. Here, we also conduct experiment to show its effectiveness. Specifically, we train our model on LOL dataset without data augmentation, and record the result in Table 6. As can be seen from the table, the proposed data augmentation strategy can facilitate to the overall performance, especially for the SSIM metric.

4.4 Failure Cases

Although achieved promising performance in the experiments, our method still has its limitations,

especially under some real challenging scenarios. Here we show two typical failure cases of our method in Fig. 14, for which the enhanced images are still unsatisfactory. The first image in Fig. 14 is with extremely low light intensity, and a lot of detail information in the dark area is lost. Consequently, our method fails to lighten the dark area of the image. In comparison, the second image in the figure is with extremely non-homogeneous light conditions in different regions and our method produces a distorted result.

5 Conclusions

In this work, we have proposed a new deep learning framework, following a decomposition-adjustment pipeline based on Retinex theory, called RAUNA, for the LIE problem. Specifically, for decomposition, we have designed a Retinex decomposition network inspired by unrolling an algorithm for solving the optimization based Retinex decomposition, with both explicit and implicit priors; for adjustment, we have presented simple yet effective structures by considering both global brightness and local brightness sensitivity. To avoid manually parameter tuning, a self-supervised fine-tuning strategy has also been adopted. Experiments on a series of typical datasets have demonstrated the effectiveness of the proposed RAUNA method, as compared with existing ones. In the future, we will devote to addressing more complex degradations for images captured in real low-light conditions, e.g., the failure cases shown in Fig. 14.

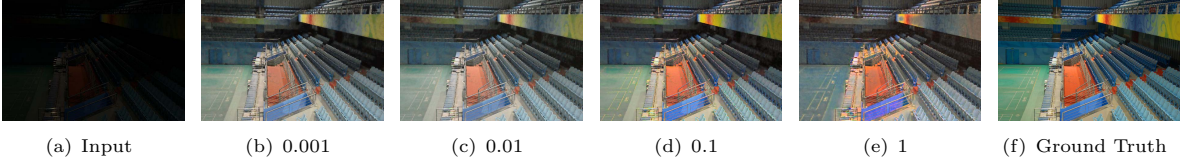


Fig. 13 Visual comparison of using different values of weight γ for the structure-revealing prior in (6).



Fig. 14 Two typical failure examples based on our model. The first and second columns are the input low-light images, and the third and fourth column are the corresponding enhanced images by our method.

Appendix A Calculations of the Descent Directions in Algorithm 1

A.1 Calculations of $d_{\mathbf{L}}$

As summarized in Eq. (9) of the main text,

$$d_{\mathbf{L}} = (\nabla^2 f_1(\mathbf{L}))^{-1} \nabla f_1(\mathbf{L}), \quad (\text{A1})$$

where

$$f_1(\mathbf{L}) = \frac{1}{2} \|\mathbf{I} - \mathbf{R} \circ \mathbf{L}\|_F^2. \quad (\text{A2})$$

Reshaping matrix to vector, the above equations can be equivalently rewritten as

$$d_{\mathbf{l}} = (\nabla^2 f_1(\mathbf{l}))^{-1} \nabla f_1(\mathbf{l}), \quad (\text{A3})$$

and

$$f_1(\mathbf{l}) = \frac{1}{2} \|\mathbf{i} - \mathbf{r} \circ \mathbf{l}\|_2^2, \quad (\text{A4})$$

respectively, where $\mathbf{i}, \mathbf{l}, \mathbf{r}$ are the vector forms of $\mathbf{I}, \mathbf{L}, \mathbf{R}$. Then the gradient of $f_1(\mathbf{l})$ can be calculated as

$$\nabla f_1(\mathbf{l}) = \mathbf{r} \circ (\mathbf{r} \circ \mathbf{l} - \mathbf{i}), \quad (\text{A5})$$

and the Hessian matrix can be further calculated as

$$\nabla^2 f_1(\mathbf{l}) = \text{diag}(\mathbf{r} \circ \mathbf{r}), \quad (\text{A6})$$

where $\text{diag}(\mathbf{x})$ denotes the diagonal matrix with the diagonal elements being vector \mathbf{x} . Substituting

$\nabla f_1(\mathbf{l})$ and $\nabla^2 f_1(\mathbf{l})$ by (A5) and (A6) in (A3), we can get

$$d_{\mathbf{l}} = (\text{diag}(\mathbf{r} \circ \mathbf{r}))^{-1} \mathbf{r} \circ (\mathbf{r} \circ \mathbf{l} - \mathbf{i}). \quad (\text{A7})$$

Since $\text{diag}(\mathbf{r} \circ \mathbf{r})$ is a diagonal matrix, then the above equation can be further written as

$$d_{\mathbf{l}} = \mathbf{r} \circ (\mathbf{r} \circ \mathbf{l} - \mathbf{i}) \oslash (\mathbf{r} \circ \mathbf{r}), \quad (\text{A8})$$

which can finally be reshaped back to matrix as

$$d_{\mathbf{L}} = (\mathbf{R} \circ (\mathbf{R} \circ \mathbf{L} - \mathbf{I})) \oslash (\mathbf{R} \circ \mathbf{R}), \quad (\text{A9})$$

by noting that all the involved operations are performed element-wise.

A.2 Calculations of $d_{\mathbf{R}}$

According to Eq. (12) of the main text,

$$d_{\mathbf{R}} = (\nabla^2 f_2(\mathbf{R}))^{-1} \nabla f_2(\mathbf{R}), \quad (\text{A10})$$

where

$$f_2(\mathbf{R}) = \frac{1}{2} \|\mathbf{I} - \mathbf{R} \circ \mathbf{L}\|_F^2 + \frac{\gamma}{4} \sum_{i=x,y} \|\mathbf{d}_i \otimes \mathbf{R} - \mathbf{G}_i\|_F^2. \quad (\text{A11})$$

Similar as that for calculating $d_{\mathbf{L}}$, we can equivalently rewrite the above equations with respect to vectors:

$$d_{\mathbf{r}} = (\nabla^2 f_2(\mathbf{r}))^{-1} \nabla f_2(\mathbf{r}), \quad (\text{A12})$$

$$f_2(\mathbf{r}) = \frac{1}{2} \|\mathbf{i} - \mathbf{r} \circ \mathbf{l}\|_2^2 + \frac{\gamma}{4} \sum_{i=x,y} \|\mathbf{D}_i \mathbf{r} - \mathbf{g}_i\|_2^2, \quad (\text{A13})$$

where $\mathbf{D}_i \mathbf{r}$ is the matrix-vector representation of the convolution $\mathbf{d}_i \otimes \mathbf{R}$ defined in Eq. (6) of the main text, with \mathbf{D}_i being the difference operator matrix with respect to \mathbf{d}_i , and \mathbf{g}_i is the vectorization of \mathbf{G}_i , also defined in Eq. (6) of the main

text. Similar as before, the gradient and Hessian of $f_2(\mathbf{r})$ with respect to \mathbf{r} can be calculated as

$$\nabla f_2(\mathbf{r}) = \mathbf{1} \circ (\mathbf{r} \circ \mathbf{1} - \mathbf{i}) + \frac{\gamma}{2} \sum_{i=x,y} \mathbf{D}_i^\top (\mathbf{D}_i \mathbf{r} - \mathbf{g}_i), \quad (\text{A14})$$

and

$$\nabla^2 f_2(\mathbf{r}) = \text{diag}(\mathbf{1} \circ \mathbf{1}) + \frac{\gamma}{2} \sum_{i=x,y} \mathbf{D}_i^\top \mathbf{D}_i, \quad (\text{A15})$$

respectively. Since $\nabla^2 f_2(\mathbf{r})$ now is not a diagonal matrix, the calculating of $d_{\mathbf{R}}$ is problematic due to the involved matrix inversion. Therefore, we resort to a diagonal approximation to $\nabla^2 f_2(\mathbf{r})$, such that the matrix inversion can be done elementwise as that for calculating $\nabla^2 f_1(\mathbf{l})$. Specifically, considering the eigenvalues of $\mathbf{D}_i^\top \mathbf{D}_i$ are upper-bounded by 4, by virtue of the property of difference operator matrix, we have

$$\text{diag}(\mathbf{1} \circ \mathbf{1}) + 4\gamma \mathbf{F} \succeq \nabla^2 f_2(\mathbf{r}), \quad (\text{A16})$$

where \mathbf{F} is the identity matrix, and $\mathbf{A} \succeq \mathbf{B}$ means that $\mathbf{A} - \mathbf{B}$ is a positive semi-definite matrix. Consequently, we can approximate the Hessian $\nabla^2 f_2(\mathbf{r})$ by

$$\nabla^2 f_2(\mathbf{r}) \approx \text{diag}(\mathbf{1} \circ \mathbf{1}) + 4\gamma \mathbf{F}, \quad (\text{A17})$$

which then results in a quasi-Newton approximation to the exactly Newton descent direction d_r :

$$d_r \approx \left(\mathbf{1} \circ (\mathbf{r} \circ \mathbf{1} - \mathbf{i}) + \frac{\gamma}{2} \sum_{i=x,y} \mathbf{D}_i^\top (\mathbf{D}_i \mathbf{r} - \mathbf{g}_i) \right) \circ (\text{diag}(\mathbf{1} \circ \mathbf{1}) + 4\gamma \mathbf{F}). \quad (\text{A18})$$

Rewriting d_r with matrix form, we can finally get

$$d_{\mathbf{R}} \approx \left((\mathbf{R} \circ \mathbf{L} - \mathbf{I}) \circ \mathbf{L} + \frac{\gamma}{2} \sum_{i=x,y} \mathbf{d}_i \otimes^\top (\mathbf{d}_i \otimes \mathbf{R} - \mathbf{G}_i) \right) \circ (\mathbf{L} \circ \mathbf{L} + 4\gamma \mathbf{E}). \quad (\text{A19})$$

References

- Acharya, T., & Ray, A.K. (2005). *Image processing: principles and applications*. John Wiley & Sons.
- Boyd, S., & Vandenberghe, L. (2004). *Convex optimization*. Cambridge university press.
- Bychkovsky, V., Paris, S., Chan, E., Durand, F. (2011). Learning photographic global tonal adjustment with a database of input / output image pairs. *The twenty-fourth ieee conference on computer vision and pattern recognition*.
- Chen, Z., Wang, Y., Yang, Y., Liu, D. (2021). Psd: Principled synthetic-to-real dehazing guided by physical priors. *Proceedings of the ieee/cvf conference on computer vision and pattern recognition* (pp. 7180–7189).
- Dabov, K., Foi, A., Katkovnik, V., Egiazarian, K. (2007). Image denoising by sparse 3-d transform-domain collaborative filtering. *IEEE Transactions on image processing*, 16(8), 2080–2095.
- Dong, C., Loy, C.C., He, K., Tang, X. (2015). Image super-resolution using deep convolutional networks. *IEEE transactions on pattern analysis and machine intelligence*, 38(2), 295–307.
- Fan, M., Wang, W., Yang, W., Liu, J. (2020). Integrating semantic segmentation and retinex model for low-light image enhancement. *Proceedings of the 28th acm international conference on multimedia* (pp. 2317–2325).
- Fu, X., Zeng, D., Huang, Y., Zhang, X.-P., Ding, X. (2016, June). A weighted variational model for simultaneous reflectance and illumination estimation. *Proceedings of the ieee conference on computer vision and pattern recognition (cvpr)*.
- Guan, X., Jian, S., Hongda, P., Zhiguo, Z., Haibin, G. (2009). An image enhancement method based on gamma correction. *2009 second international symposium on computational intelligence and design* (Vol. 1, pp. 60–63).
- Guo, C., Li, C., Guo, J., Loy, C.C., Hou, J., Kwong, S., Cong, R. (2020). Zero-reference deep curve estimation for low-light image

- enhancement. *Proceedings of the ieee/cvf conference on computer vision and pattern recognition* (pp. 1780–1789).
- Guo, X. (2016). Lime: a method for low-light image enhancement. *Proceedings of the 24th acm international conference on multimedia* (pp. 87–91).
- He, K., Zhang, X., Ren, S., Sun, J. (2016). Deep residual learning for image recognition. *Proceedings of the ieee conference on computer vision and pattern recognition* (pp. 770–778).
- Huang, S.-C., Cheng, F.-C., Chiu, Y.-S. (2012). Efficient contrast enhancement using adaptive gamma correction with weighting distribution. *IEEE transactions on image processing*, 22(3), 1032–1041.
- Hummel, R. (1977). Image enhancement by histogram transformation. *Computer Graphics and Image Processing*, 6(2), 184–195.
- Jiang, Y., Gong, X., Liu, D., Cheng, Y., Fang, C., Shen, X., ... Wang, Z. (2021). Enlighten-gan: Deep light enhancement without paired supervision. *IEEE Transactions on Image Processing*, 30, 2340–2349.
- Jobson, D.J., Rahman, Z.-u., Woodell, G.A. (1997). Properties and performance of a center/surround retinex. *IEEE transactions on image processing*, 6(3), 451–462.
- Johnson, J., Alahi, A., Fei-Fei, L. (2016). Perceptual losses for real-time style transfer and super-resolution. B. Leibe, J. Matas, N. Sebe, & M. Welling (Eds.), *Proceedings of the european conference on computer vision (eccv)* (p. 694–711). Cham: Springer International Publishing.
- Kim, Y.-T. (1997). Contrast enhancement using brightness preserving bi-histogram equalization. *IEEE transactions on Consumer Electronics*, 43(1), 1–8.
- Kingma, D.P., & Ba, J. (2015). Adam: A method for stochastic optimization. Y. Bengio & Y. LeCun (Eds.), *3rd international conference on learning representations*.
- Land, E.H. (1977). The retinex theory of color vision. *Scientific american*, 237(6), 108–129.
- Ledig, C., Theis, L., Huszár, F., Caballero, J., Cunningham, A., Acosta, A., ... Shi, W. (2017). Photo-realistic single image super-resolution using a generative adversarial network. *2017 ieee conference on computer vision and pattern recognition (cvpr)* (p. 105–114). 10.1109/CVPR.2017.19
- Lee, C., Lee, C., Kim, C.-S. (2013). Contrast enhancement based on layered difference representation of 2d histograms. *IEEE transactions on image processing*, 22(12), 5372–5384.
- Li, C., Guo, C.G., Loy, C.C. (2021). Learning to enhance low-light image via zero-reference deep curve estimation. *Ieee transactions on pattern analysis and machine intelligence*. 10.1109/TPAMI.2021.3063604
- Li, C., Guo, J., Porikli, F., Pang, Y. (2018). Lightnet: A convolutional neural network for weakly illuminated image enhancement. *Pattern recognition letters*, 104, 15–22.
- Li, L., Wang, R., Wang, W., Gao, W. (2015). A low-light image enhancement method for both denoising and contrast enlarging. *2015 ieee international conference on image processing (ICIP)* (pp. 3730–3734).
- Li, M., Liu, J., Yang, W., Sun, X., Guo, Z. (2018a). Structure-revealing low-light image enhancement via robust retinex model. *IEEE Transactions on Image Processing*, 27(6), 2828–2841.
10.1109/TIP.2018.2810539

- Li, M., Liu, J., Yang, W., Sun, X., Guo, Z. (2018b). Structure-revealing low-light image enhancement via robust retinex model. *IEEE Transactions on Image Processing*, 27(6), 2828–2841.
- Lim, S., & Kim, W. (2020). Dslr: Deep stacked laplacian restorer for low-light image enhancement. *IEEE Transactions on Multimedia*.
- Liu, J., Xu, D., Yang, W., Fan, M., Huang, H. (2021, Apr 01). Benchmarking low-light image enhancement and beyond. *International Journal of Computer Vision*, 129(4), 1153–1184. Retrieved from <https://doi.org/10.1007/s11263-020-01418-8>
- 10.1007/s11263-020-01418-8
- Liu, R., Ma, L., Zhang, J., Fan, X., Luo, Z. (2021). Retinex-inspired unrolling with cooperative prior architecture search for low-light image enhancement. *Proceedings of the IEEE/CVF conference on computer vision and pattern recognition* (pp. 10561–10570).
- Lore, K.G., Akintayo, A., Sarkar, S. (2017). Llnet: A deep autoencoder approach to natural low-light image enhancement. *Pattern Recognition*, 61, 650–662.
- <https://doi.org/10.1016/j.patcog.2016.06.008>
- Lu, K., & Zhang, L. (2020). Tbefn: A two-branch exposure-fusion network for low-light image enhancement. *IEEE Transactions on Multimedia*.
- Lv, F., Liu, B., Lu, F. (2020). Fast enhancement for non-uniform illumination images using light-weight cnns. *Proceedings of the 28th acm international conference on multimedia* (pp. 1450–1458).
- Lv, F., Lu, F., Wu, J., Lim, C. (2018). MBLLEN: Low-light image/video enhancement using CNNs. *British machine vision conference (bmvc)*.
- Ma, L., Liu, R., Zhang, J., Fan, X., Luo, Z. (2021). Learning deep context-sensitive decomposition for low-light image enhancement. *IEEE Transactions on Neural Networks and Learning Systems*.
- Mittal, A., Soundararajan, R., Bovik, A.C. (2013). Making a “completely blind” image quality analyzer. *IEEE Signal Processing Letters*, 20(3), 209–212.
- 10.1109/LSP.2012.2227726
- Narasimhan, S.G., & Nayar, S.K. (2002, Jul 01). Vision and the atmosphere. *International Journal of Computer Vision*, 48(3), 233–254. Retrieved from <https://doi.org/10.1023/A:1016328200723>
- 10.1023/A:1016328200723
- Parikh, N., & Boyd, S. (2014, jan). Proximal algorithms. *Found. Trends Optim.*, 1(3), 127–239. Retrieved from <https://doi.org/10.1561/2400000003>
- 10.1561/2400000003
- Pisano, E.D., Zong, S., Hemminger, B.M., DeLuca, M., Johnston, R.E., Muller, K., ... Pizer, S.M. (1998). Contrast limited adaptive histogram equalization image processing to improve the detection of simulated spiculations in dense mammograms. *Journal of Digital Imaging*, 11(4), 193.
- Pizer, S.M., Amburn, E.P., Austin, J.D., Cromartie, R., Geselowitz, A., Greer, T., ... Zuiderveld, K. (1987). Adaptive histogram equalization and its variations. *Computer vision, graphics, and image processing*, 39(3), 355–368.
- Rahman, Z., Jobson, D.J., Woodell, G.A. (1996). Multi-scale retinex for color image enhancement. *Proceedings of 3rd IEEE international*

conference on image processing (Vol. 3, pp. 1003–1006).

- Ren, X., Yang, W., Cheng, W.-H., Liu, J. (2020). Lr3m: Robust low-light enhancement via low-rank regularized retinex model. *IEEE Transactions on Image Processing*, 29, 5862–5876.
- 10.1109/TIP.2020.2984098
- Reza, A.M. (2004). Realization of the contrast limited adaptive histogram equalization (clahe) for real-time image enhancement. *Journal of VLSI signal processing systems for signal, image and video technology*, 38(1), 35–44.
- Shen, L., Yue, Z., Feng, F., Chen, Q., Liu, S., Ma, J. (2017). Msr-net: Low-light image enhancement using deep convolutional network. *arXiv preprint arXiv:1711.02488*.
- Simonyan, K., & Zisserman, A. (2014). Very deep convolutional networks for large-scale image recognition. *arXiv preprint arXiv:1409.1556*.
- Singh, H., Kumar, A., Balyan, L.K., Singh, G.K. (2017). A novel optimally gamma corrected intensity span maximization approach for dark image enhancement. *2017 22nd international conference on digital signal processing (dsp)* (p. 1-5). 10.1109/ICDSP.2017.8096035
- Sun, C.-C., Ruan, S.-J., Shie, M.-C., Pai, T.-W. (2005). Dynamic contrast enhancement based on histogram specification. *IEEE Transactions on Consumer Electronics*, 51(4), 1300–1305.
- Sun, Y., Wang, X., Liu, Z., Miller, J., Efros, A., Hardt, M. (2020, 13–18 Jul). Test-time training with self-supervision for generalization under distribution shifts. H.D. III & A. Singh (Eds.), *Proceedings of the 37th international conference on machine learning* (Vol. 119, pp. 9229–9248). PMLR.
- Ulyanov, D., Vedaldi, A., Lempitsky, V. (2018). Deep image prior. *Proceedings of the IEEE conference on computer vision and pattern recognition* (pp. 9446–9454).
- Wang, H., Xie, Q., Zhao, Q., Meng, D. (2020). A model-driven deep neural network for single image rain removal. *2020 IEEE/CVF Conference on Computer Vision and Pattern Recognition (CVPR)* (p. 3100–3109). 10.1109/CVPR42600.2020.00317
- Wang, R., Zhang, Q., Fu, C.-W., Shen, X., Zheng, W.-S., Jia, J. (2019). Underexposed photo enhancement using deep illumination estimation. *Proceedings of the IEEE/CVF Conference on Computer Vision and Pattern Recognition* (pp. 6849–6857).
- Wang, S., Zheng, J., Hu, H.-M., Li, B. (2013a). Naturalness preserved enhancement algorithm for non-uniform illumination images. *IEEE Transactions on Image Processing*, 22(9), 3538–3548.
- 10.1109/TIP.2013.2261309
- Wang, S., Zheng, J., Hu, H.-M., Li, B. (2013b). Naturalness preserved enhancement algorithm for non-uniform illumination images. *IEEE Transactions on Image Processing*, 22(9), 3538–3548.
- Wang, W., Sun, N., Ng, M.K. (2019). A variational gamma correction model for image contrast enhancement. *Inverse Problems & Imaging*, 13(3), 461–478.
- Wang, Y., Cao, Y., Zha, Z.-J., Zhang, J., Xiong, Z., Zhang, W., Wu, F. (2019a). Progressive retinex: Mutually reinforced illumination-noise perception network for low-light image enhancement. *Proceedings of the 27th ACM international conference on multimedia* (p. 2015–2023). New York, NY, USA: Association for Computing Machinery. Retrieved from

<https://doi.org/10.1145/3343031.3350983>
10.1145/3343031.3350983

Wang, Y., Cao, Y., Zha, Z.-J., Zhang, J., Xiong, Z., Zhang, W., Wu, F. (2019b). Progressive retinex: Mutually reinforced illumination-noise perception network for low-light image enhancement. *Proceedings of the 27th acm international conference on multimedia* (pp. 2015–2023).

Wang, Z., Bovik, A.C., Sheikh, H.R., Simoncelli, E.P. (2004). Image quality assessment: from error visibility to structural similarity. *IEEE transactions on image processing*, 13(4), 600–612.

Wei, C., Wang, W., Yang, W., Liu, J. (2018). Deep retinex decomposition for low-light enhancement. *British machine vision conference*.

Wu, Y., Lim, J., Yang, M.-H. (2015). Object tracking benchmark. *IEEE Transactions on Pattern Analysis and Machine Intelligence*, 37(9), 1834–1848.

10.1109/TPAMI.2014.2388226

Xie, Q., Zhou, M., Zhao, Q., Xu, Z., Meng, D. (2020). Mhf-net: An interpretable deep network for multispectral and hyperspectral image fusion. *IEEE Transactions on Pattern Analysis and Machine Intelligence*, 1-1.

10.1109/TPAMI.2020.3015691

Xu, K., Yang, X., Yin, B., Lau, R.W. (2020). Learning to restore low-light images via decomposition-and-enhancement. *Proceedings of the IEEE/CVF conference on computer vision and pattern recognition* (pp. 2281–2290).

Yang, D., & Sun, J. (2018, September). Proximal dehaze-net: A prior learning-based deep network for single image dehazing. *Proceedings of the european conference on computer vision (eccv)* (p. 729-746).

Yang, W., Wang, S., Fang, Y., Wang, Y., Liu, J. (2020). From fidelity to perceptual

quality: A semi-supervised approach for low-light image enhancement. *Proceedings of the IEEE/CVF conference on computer vision and pattern recognition* (pp. 3063–3072).

Yang, W., Wang, W., Huang, H., Wang, S., Liu, J. (2021). Sparse gradient regularized deep retinex network for robust low-light image enhancement. *IEEE Transactions on Image Processing*, 30, 2072–2086.

Yang, Y., Sun, J., Li, H., Xu, Z. (2020). Admm-csnet: A deep learning approach for image compressive sensing. *IEEE Transactions on Pattern Analysis and Machine Intelligence*, 42(3), 521-538.

10.1109/TPAMI.2018.2883941

Ypma, T.J. (1995). Historical development of the newton–raphson method. *SIAM review*, 37(4), 531–551.

Yuan, L., & Sun, J. (2012). Automatic exposure correction of consumer photographs. *European conference on computer vision* (pp. 771–785).

Zhang, J., Pan, J., Lai, W.-S., Lau, R.W.H., Yang, M.-H. (2017). Learning fully convolutional networks for iterative non-blind deconvolution. *2017 IEEE conference on computer vision and pattern recognition (cvpr)* (p. 6969-6977). 10.1109/CVPR.2017.737

Zhang, K., Zuo, W., Chen, Y., Meng, D., Zhang, L. (2017). Beyond a gaussian denoiser: Residual learning of deep cnn for image denoising. *IEEE transactions on image processing*, 26(7), 3142–3155.

Zhang, X., Shen, P., Luo, L., Zhang, L., Song, J. (2012). Enhancement and noise reduction of very low light level images. *Proceedings of the 21st international conference on pattern recognition (icpr2012)* (p. 2034-2037).

Zhang, Y., Guo, X., Ma, J., Liu, W., Zhang, J. (2021). Beyond brightening low-light

images. *International Journal of Computer Vision*, 129(4), 1013–1037.

Zhang, Y., Zhang, J., Guo, X. (2019). Kindling the darkness: A practical low-light image enhancer. *Proceedings of the 27th acm international conference on multimedia* (pp. 1632–1640).

Zhao, Z., Xiong, B., Wang, L., Ou, Q., Yu, L., Kuang, F. (2021). Retinexdip: A unified deep framework for low-light image enhancement. *IEEE Transactions on Circuits and Systems for Video Technology*.

Zhao, Z., Zheng, P., Xu, S., Wu, X. (2019). Object detection with deep learning: A review. *IEEE transactions on neural networks and learning systems*, 30(11), 3212–3232.

Zheng, C., Shi, D., Shi, W. (2021). Adaptive unfolding total variation network for low-light image enhancement. *Proceedings of the ieee/cvf international conference on computer vision* (pp. 4439–4448).

Zhu, A., Zhang, L., Shen, Y., Ma, Y., Zhao, S., Zhou, Y. (2020). Zero-shot restoration of underexposed images via robust retinex decomposition. *2020 ieee international conference on multimedia and expo (icme)* (p. 1–6). 10.1109/ICME46284.2020.9102962

Zuiderveld, K. (1994). Contrast limited adaptive histogram equalization. In *Graphics gems iv* (p. 474–485). USA: Academic Press Professional, Inc.